



Second-Order, Energy-Stable and Maximum Bound Principle Preserving Schemes for Two-Phase Incompressible Flow

Xiaoli Li¹ · Hao Liu² · Nan Zheng³

Received: 17 June 2024 / Revised: 7 December 2024 / Accepted: 11 January 2025 /
Published online: 4 February 2025
© The Author(s) 2025

Abstract

In this paper, we propose several linear fully discrete schemes for the mass-conserved Allen-Cahn-Navier-Stokes equation, based on the generalized stabilized exponential scalar auxiliary variable approach in time and the marker and cell (MAC) scheme in space. It is quite remarkable that our schemes can guarantee second-order accuracy in space provided the maximum bound principle (MBP) is satisfied, whereas most previous work can only possess first-order accuracy in space. We rigorously show that the constructed schemes satisfy the unconditional energy dissipation law and preserve the MBP. Finally, various numerical examples are presented to verify the theoretical results and demonstrate the efficiency of the proposed schemes.

Keywords Allen-Cahn · Navier-Stokes · Energy dissipation · Second-order · MAC scheme · Maximum bound principle

Mathematics Subject Classification 65M12 · 65M15 · 35K35

1 Introduction

In this paper, we study the two-phase incompressible flow [1–5]:

$$\partial_t \phi + \nabla \cdot (\mathbf{u}\phi) = -\mathcal{M}\mu, \quad \text{in } \Omega \times (0, T), \quad (1.1a)$$

$$\mu = \lambda \left(-\epsilon^2 \Delta \phi - f(\phi) + L(\phi(t)) \right), \quad \text{in } \Omega \times (0, T), \quad (1.1b)$$

✉ Hao Liu
mathhao.liu@sjtu.edu.cn

✉ Nan Zheng
nanzheng@polyu.edu.hk

Xiaoli Li
xiaolimath@sdu.edu.cn

¹ School of Mathematics, Shandong University, Jinan 250100, Shandong, China

² School of Mathematical Sciences and Institute of Natural Sciences, Shanghai Jiao Tong University, Shanghai, China

³ Department of Applied Mathematics, The Hong Kong Polytechnic University, Hung Hom, Kowloon, Hong Kong

$$\mathbf{u}_t + (\mathbf{u} \cdot \nabla) \mathbf{u} - \nu \Delta \mathbf{u} + \nabla p = \mu \nabla \phi, \quad \text{in } \Omega \times (0, T), \quad (1.1c)$$

$$\nabla \cdot \mathbf{u} = 0, \quad \text{in } \Omega \times (0, T), \quad (1.1d)$$

subject to the boundary condition

$$\frac{\partial \phi}{\partial \mathbf{n}}|_{\partial \Omega} = 0, \quad \mathbf{u}|_{\partial \Omega} = 0. \quad (1.2)$$

Here, $\Omega \subset \mathbb{R}^d$ is a smooth bounded domain, with the boundary $\partial \Omega$. The unknowns in equations (1.1a)–(1.1d) are the phase function ϕ , the chemical potential μ , the velocity \mathbf{u} , and the pressure p . The parameter $\mathcal{M} > 0$ represents the mobility, while $\epsilon > 0$ is a small constant that controls the thickness of the diffuse interface. Additionally, $\lambda > 0$ is a constant related to the surface tension, and ν denotes the fluid viscosity. The function f is the derivative of the configuration potential function F , i.e., $f = -F'$, and the nonlocal term $L(\phi(t))$ is the Lagrange multiplier, playing a crucial role in the elimination of the total mass variance $|\Omega|$ (cf. [6]). A widely adopted choice for $L(\phi(t))$ in (1.1b) is proposed in the following form:

$$L(\phi(t)) = \frac{1}{|\Omega|} \int_{\Omega} f(\phi(\mathbf{y}, t)) d\mathbf{y}, \quad \mathbf{x} \in \Omega. \quad (1.3)$$

A variety of Allen-Cahn phase-field models have been widely utilized to simulate multi-component systems, including the multi-phase fluid flow, crystal growth, membranes for vesicles, and many others. In the conserved Allen-Cahn equation, a nonlocal term is proposed to eliminate the variance in mass caused by the nonlinear term, hence ensuring the preservation of total mass. Nevertheless, the conserved Allen-Cahn model becomes a highly complex system when coupled with the Navier–Stokes equations, thereby a significant challenge lies in designing the fully decoupled, linear, and maximum bound principle (MBP) preserving scheme that also satisfies the unconditional energy dissipation law.

There are several effective methods for solving the incompressible Navier–Stokes equation and the conserved Allen-Cahn equation respectively. For the incompressible Navier–Stokes equation, Shen [7] proposed a first-order decoupled pressure-correction method and established rigorous error estimates. A unified approach on designing simple, efficient, and energy-stable time discretization schemes for the two-phase incompressible flow with matching or non-matching density has been presented in [8]. As for solving the phase-field model, various methods that preserve the energy dissipation law are used, such as linear stabilization [9], convex splitting method [10, 11], invariant energy quadratization [12, 13], and scalar auxiliary variable approach [14, 15].

We would like to point out that, in addition to energy stability, MBP is another crucial property of the conserved Allen-Cahn equation. A popular method preserving the MBP for the convective Allen-Cahn equation has been studied by using the upwind strategy for spatial discretization. In a previous study [16], a first-order numerical scheme was developed for the conserved Allen-Cahn equation, demonstrating the unconditional preservation of MBP by employing the upwind finite difference method. Recently, Cai et al. [17] extended this approach and constructed the first- and second-order in time unconditionally MBP-preserving upwind exponential time differencing (ETD) schemes. However, the upwind strategy only achieves first-order accuracy in space and requires strict CFL stability conditions, making it difficult to capture the dynamical interface behavior of the phase evolution in practice. Furthermore, in [18], the convective Allen-Cahn equation is split into a mass-conserving Allen-Cahn equation and a transport equation using the operator splitting approach. For the coupled conserved Allen-Cahn–Navier–Stokes equation, Huang, Lin, and Ardekani [19] developed a consistent and conservative scheme that ensures the mass and the momentum

conservation while satisfying the energy law of the two-phase system. Moreover, Yang [5] constructed a fully decoupled scheme that is linear, unconditional energy stable, and second-order-in time accurate.

As far as we know, despite that a significant amount of work has been dedicated to the construction and analysis of the computational schemes to the conserved Allen-Cahn-Navier-Stokes (ACNS) system, there is still no fully decoupled, linear, high-order-in-time, unconditionally energy decay, and MBP preserving scheme. The objective of this study is to develop high-order and efficient numerical schemes for solving the hydrodynamically coupled mass-conserved Allen-Cahn phase-field model in a two-phase fluid flow system. The work presented in this paper is unique in the following aspects:

- We construct first- and second-order in time, second-order in space, linear and fully decoupled schemes for the conserved ACNS model, ensuring unconditional energy stable through on the generalized stabilized exponential scalar auxiliary variable approach [20, 21].
- The MBP properties of the Allen-Cahn equation with multipliers (1.3) under different potential function $F(\phi)$ are rigorously proved. The main innovation of the proof is treating the nonlocal equation as a semi-linear parabolic equation with given coefficients, allowing us to utilize the strong maximum (comparison) principle and Hopf's boundary point lemma for the parabolic equations and the special properties of the energy. This proof is quite concise, robust, and can be easily extended to a broader range of multipliers.
- We derive the corresponding MBP for the developed first- and second-order numerical schemes in time based on the second-order MAC scheme in space rigorously. By establishing a unified framework under some reasonable assumptions [22, 23], we prove that the second-order spatial central difference method can still preserves the MBP.

To the best of the authors' knowledge, this is the first linear, second-order accuracy in space and time, energy decay, and MBP-preserving numerical scheme for a two-phase fluid flow system.

The rest of this paper is organized as follows. In Sect. 2, we present some preliminaries and show the maximum bound principle for the nonlocal ACNS model and introduce some notations for the discretized problem. In Sect. 3, we propose the first- and second-order stabilized generalized exponential scalar auxiliary variable schemes, demonstrating their adherence to the unconditional energy dissipation law and the MBP. Numerical experiments are carried out to validate the theoretical results and demonstrate the performance of the proposed schemes in Sect. 4. Finally, some concluding remarks are given in Sect. 5.

2 The Problem Description and Notations

In this section, we first derive the energy dissipation law and the maximum bound principle (MBP) [24, 25] for the ACNS model (1.1). Following that, some preliminaries and notations will be presented below, which will be utilized throughout the paper.

The ACNS Eq. (1.1) with a nonlocal constraint satisfies an energy dissipation law. Indeed, taking the inner products of (1.1a) with μ , (1.1b) with $\partial_t \phi$, and (1.1c) with \mathbf{u} respectively, summing them up yields the following energy dissipation law

$$\frac{d}{dt} \mathcal{E}(\phi, \mathbf{u}) = - \int_{\Omega} \mathcal{M} |\mu|^2 + \nu |\nabla \mathbf{u}|^2 d\mathbf{x},$$

where

$$\mathcal{E}(\phi, \mathbf{u}) = \int_{\Omega} \left(\lambda \left(\frac{\epsilon^2}{2} |\nabla \phi|^2 + F(\phi) \right) + \frac{1}{2} |\mathbf{u}|^2 \right) d\mathbf{x}.$$

We impose the following assumption on f , which will be used in establishing the MBP for (1.1) with $L(\phi)$ given in (1.3); see Proposition 2.1.

Assumption 1 The function $f : \mathbb{R} \rightarrow \mathbb{R}$ is continuously differentiable and there exists some $\beta > 0$ such that

$$f(\beta) \leq f(x) \leq f(-\beta), \quad -\beta \leq x \leq \beta. \quad (2.4)$$

We consider two common forms of the function $F(\phi)$ used in phase-field modelling. The first one is the double-well structure, which can be expressed as

$$F(\phi) = \frac{1}{4}(\phi^2 - 1)^2. \quad (2.5)$$

The second form is the Flory-Huggins potential function, given by

$$F(\phi) = \frac{\theta}{2}[(1 + \phi) \ln(1 + \phi) + (1 - \phi) \ln(1 - \phi)] - \frac{\theta_c}{2}\phi^2, \quad (2.6)$$

where $0 < \theta < \theta_c$.

Given a terminal time $T > 0$, we can deduce that the ACNS Eq. (1.1) satisfies the MBP under Assumption 1. We note that the MBP holds with different values of the maximum bounds depending on the choice of the function F in $L(\phi(t))$ in (1.3).

Proposition 2.1 Let $\mathbf{u} \in C([0, T]; [C^1(\Omega)]^d)$ and $\phi \in C^1([0, T]; C^2(\Omega))$ be the solution to model (1.1) with $L(\phi(t))$ given by (1.3). Suppose that f satisfies Assumption 1. Then the MBP holds, precisely, if the initial data satisfies $\|\phi_0\|_{\infty} < \beta$, where β is determined by (2.4), then for any $t \in [0, T]$, we have

$$\|\phi(\cdot, t)\|_{\infty} \leq \beta.$$

Proof Let $L(t) = \frac{1}{|\Omega|} \int_{\Omega} f(\phi(\mathbf{y}, t)) d\mathbf{y}$. We then consider the following operator

$$\mathcal{S}(h) := \partial_t h + \nabla \cdot (\mathbf{u}h) + \lambda \mathcal{M}(-\epsilon^2 \Delta h - f(h)).$$

Obviously, $\mathcal{S}(\phi)(x, t) = -\lambda \mathcal{M}L(t)$. Moreover, we define

$$t^* = \sup\{0 \leq t \leq T; \sup_{0 \leq s \leq t} \|\phi(\cdot, s)\|_{L^{\infty}(\bar{\Omega})} \leq \beta\}.$$

Then direct calculations together with (1.1d), i.e., $\nabla \cdot \mathbf{u} = 0$ and (2.4) the assumption on f show that on $[0, t^*] \times \bar{\Omega}$, we have

$$\mathcal{S}(\beta) = -\lambda \mathcal{M}f(\beta) \geq -\lambda \mathcal{M}L(t) = \mathcal{S}(\phi), \quad \mathcal{S}(-\beta) = -\lambda \mathcal{M}f(-\beta) \leq -\lambda \mathcal{M}L(t) = \mathcal{S}(\phi).$$

The comparison principle [26] indicates that we only have three cases

$$-\beta < \phi(\cdot, t^*) < \beta \text{ on } \Omega \text{ or } \phi(\cdot, t^*) \equiv \beta \text{ on } \Omega, \text{ or } \phi(\cdot, t^*) \equiv -\beta \text{ on } \Omega. \quad (2.7)$$

In the last two cases, by the uniqueness of the solution, we would have $\phi(\mathbf{x}, t) \equiv \beta$, or $\phi(\mathbf{x}, t) \equiv -\beta$ for $t \in [t^*, T]$, since $\phi(\mathbf{x}, t) \equiv \pm\beta$ for $t \in [t^*, T]$ is another solution to (1.1) with $\phi(x, t^*) = \pm\beta$. This contradicts the definition of t^* unless $t^* = T$. Hence, we may assume $-\beta < \phi(\cdot, t^*) < \beta$ on Ω . We further claim that

$$-\beta < \phi(\cdot, t^*) < \beta \text{ on } \bar{\Omega}. \quad (2.8)$$

Otherwise, we have for some $x \in \partial\Omega$ such that $\phi(x, t^*) = \beta$ or $\phi(x, t^*) = -\beta$. Now by Hopf's boundary point lemma, we have

$$\frac{\partial\phi(x, t^*)}{\partial\mathbf{n}} > 0 \text{ or } \frac{\partial\phi(x, t^*)}{\partial\mathbf{n}} < 0 \text{ respectively.}$$

This contradicts with the boundary condition (1.2). Hence, (2.8) holds. Then we can extend t^* to a larger value if $t^* < T$, which is a contraction. This finishes the proof. \square

Remark 2.1 The values of β rely on the specific form of the function $f = -F'$ and may not be unique. In the case F being the double well potential, β can be taken as any value in $[\frac{2\sqrt{3}}{3}, +\infty)$. On the other hand, when F is the Flory-Huggins potential, we can choose $\beta \in (\rho, 1)$ (cf. [27]), where ρ is the positive root of $f(\rho) = -F'(\rho)$.

Remark 2.2 An alternative modification for the ACNS model (1.1) is to adopt the Lagrange multiplier introduced by Brassel and Bretin (cf. [28–31]), which can be formulated as follows:

$$L(\phi(t)) = \frac{\int_{\Omega} f(\phi(\mathbf{y}, t)) d\mathbf{y}}{\int_{\Omega} \sqrt{4F(\phi(\mathbf{y}, t))} d\mathbf{y}} \sqrt{4F(\phi(\mathbf{x}, t))}, \quad \mathbf{x} \in \Omega. \quad (2.9)$$

In this case, we modify the Flory-Huggins potential by a constant as $\tilde{F}(\phi) := F(\phi) + C$, where $0 < \theta < \theta_c$ and $C = C(\theta, \theta_c)$ is chosen such that $\min_{-1 < \phi < 1} \tilde{F}(\phi) = 0$. It is easy to see that $C = -\theta[(1 + \rho)\ln(1 + \rho) + (1 - \rho)\ln(1 - \rho)]/2 + \theta_c\rho^2/2$, where ρ is the positive root of $f(\rho) = -\tilde{F}'(\rho)$. Furthermore, we can show that $\rho \in (\sqrt{1 - \theta/\theta_c}, 1)$. It follows that $\min_{-1 < \phi < 1} \tilde{F}(\phi) = \tilde{F}(\rho) = \tilde{F}(-\rho) = 0$. The same proof technique used in Proposition 2.1 applies equally well here to demonstrate that the solutions to this new model also satisfy the MBP but with a different maximum bound. In this case, we do not rely on the Assumption 1. Indeed, treating $\int_{\Omega} f(\phi(\mathbf{y}, t)) d\mathbf{y} / \int_{\Omega} \sqrt{4F(\phi(\mathbf{y}, t))} d\mathbf{y}$ as a given coefficient, the nonlocal Eq. (1.1a) can be viewed as a semi-linear equation. Now the key is to note the fact that $F(1) = 0$ for the double well potential (2.5) and $\tilde{F}(\rho) = 0$ for the modified Flory-Huggins potential, then we can apply the comparison principle and Hopf's boundary point lemma to show that the MBP holds with the corresponding bounds 1 and ρ respectively in this case.

In order to preserve the MBP of the numerical solution, we rewrite the Eq. (1.1) into an equivalent form with a stabilizing constant $\kappa > 0$,

$$\partial_t \phi + \mathbf{u} \cdot \nabla \phi = -\mathcal{M}\mu, \quad \text{in } \Omega \times (0, T), \quad (2.10a)$$

$$\mu = -\lambda(\epsilon^2 \Delta - \kappa)\phi - \lambda(\tilde{f}(\phi) + \kappa\phi), \quad \text{in } \Omega \times (0, T), \quad (2.10b)$$

$$\mathbf{u}_t + \gamma(\mathbf{u} \cdot \nabla)\mathbf{u} - \nu \Delta \mathbf{u} + \nabla p = \mu \nabla \phi, \quad \text{in } \Omega \times (0, T), \quad (2.10c)$$

$$\nabla \cdot \mathbf{u} = 0, \quad \text{in } \Omega \times (0, T), \quad (2.10d)$$

where $\tilde{f}(\phi) = f(\phi) - L(\phi(t))$ and $L(\phi(t))$ is defined in (1.3). Moreover, the stabilizing constant κ is assumed to satisfy

$$\kappa \geq \|\tilde{f}'(\xi)\|_{C[-\beta, \beta]}. \quad (2.11)$$

Lemma 2.1 ([16]) Let $B \in \mathcal{R}^{N,N}$ and $A = aI - B$, where $a > 0$ is a constant. If $B = (b_{ij})$ is a negative diagonally dominant matrix, i.e., $b_{ii} < 0$, $b_{ii} + \sum_{j \neq i} |b_{ij}| \leq 0$, for all i , then A is invertible and its inverse satisfies $\|A^{-1}\|_{L^\infty(\Omega)} \leq \frac{1}{a}$.

Lemma 2.2 ([18]) Under Assumption 1 and the condition $\kappa \geq \|\bar{f}'(\xi)\|_{C[-\beta, \beta]}$, we obtain that $|\bar{f}(\xi) + \kappa\xi| \leq \kappa\beta$ for any $\xi \in [-\beta, \beta]$.

Recalling Proposition 2.1 and noting the fact that $F(\phi)$ is bounded from below on $[-\beta, \beta]$, it holds that

$$-C_* \leq E_1(\phi(t)) = \int_{\Omega} \lambda F(\phi(t)) d\mathbf{x} \leq C^*.$$

for some constants $C_*, C^* \geq 0$.

If we introduce an SAV $s(t) = E_1(\phi(t))$, and recast the governing system (1.1) as the following

$$\begin{aligned} \partial_t \phi + \xi \mathbf{u} \cdot \nabla \phi &= -\mathcal{M}\mu, \\ \mu &= -\lambda(\epsilon^2 \Delta \phi + \xi \bar{f}(\phi)) + \kappa \lambda \xi (\phi - \phi), \\ \mathbf{u}_t + \xi (\mathbf{u} \cdot \nabla) \mathbf{u} - \nu \Delta \mathbf{u} + \nabla p &= \mu \nabla \phi, \\ \nabla \cdot \mathbf{u} &= 0, \\ s_t &= \int_{\Omega} -\mu \nabla \phi \cdot \mathbf{u} - \xi (\lambda \bar{f}(\phi) \phi_t - \gamma \mathbf{u} \cdot \nabla \mathbf{u} \cdot \mathbf{u} - \nabla \cdot (\mathbf{u} \phi) \mu) d\mathbf{x}, \end{aligned}$$

where

$$\xi = \frac{\sigma(s)}{\sigma(E_1(\phi, \mathbf{u}))}, \quad (2.12)$$

then we have the following energy form which is equivalent to $\mathcal{E}(\phi)$

$$E(\phi, \mathbf{u}, s) = \int_{\Omega} \left(\frac{\lambda \epsilon^2}{2} |\nabla \phi|^2 + \frac{1}{2} |\mathbf{u}|^2 \right) d\mathbf{x} + s \geq -C_*.$$

Here, $\sigma : \mathbb{R} \rightarrow \mathbb{R}$ is a function that satisfies the following two conditions:

- (a) $\sigma > 0$ for all $x \in \mathbb{R}$;
- (b) σ is continuously differentiable and $\sigma' \geq 0$ for all $x \in \mathbb{R}$.

These conditions play a crucial role in preserving the MBP of the numerical schemes proposed in this paper.

Remark 2.3 Some nontrivial choices for the function σ can be found in [32].

We now introduce some standard notations. The two-dimensional domain Ω is partitioned as $\Omega_x \times \Omega_y$, where

$$\begin{aligned} \Omega_x : 0 &= x_0 < x_1 < \cdots < x_{N_x-1} < x_{N_x} = L_x, \\ \Omega_y : 0 &= y_0 < y_1 < \cdots < y_{N_y-1} < y_{N_y} = L_y. \end{aligned}$$

Additionally, we use the following notations:

$$\begin{cases} x_{-1/2} = x_0 = 0, & x_{N_x+1/2} = x_{N_x} = L_x, \\ y_{-1/2} = y_0 = 0, & y_{N_y+1/2} = y_{N_y} = L_y. \end{cases}$$

For possible integers i, j , $0 \leq i \leq N_x$, $0 \leq j \leq N_y$, we define

$$\begin{aligned} x_{i+1/2} &= \frac{x_i + x_{i+1}}{2}, & h_x &= x_{i+1} - x_i = x_{i+1/2} - x_{i-1/2}, \\ y_{j+1/2} &= \frac{y_j + y_{j+1}}{2}, & h_y &= y_{j+1} - y_j = y_{j+1/2} - y_{j-1/2}, \\ \Omega_{i+1/2, j+1/2} &= (x_i, x_{i+1}) \times (y_j, y_{j+1}). \end{aligned}$$

For a function $f(x, y)$, let $f_{l,m}$ denote $f(x_l, y_m)$ where l may take values $i, i + 1/2$ and m may take values $j, j + 1/2$ for integers i, j , $0 \leq i \leq N_x$, $0 \leq j \leq N_y$. For discrete functions $f_{l,m}$ with values at proper nodal points, define

$$\begin{cases} [d_x f]_{i+1/2,m} = \frac{f_{i+1,m} - f_{i,m}}{h_x}, & [D_y f]_{l,j+1} = \frac{f_{l,j+3/2} - f_{l,j+1/2}}{h_y}, \\ [D_x f]_{i+1,m} = \frac{f_{i+3/2,m} - f_{i+1/2,m}}{h_x}, & [d_y f]_{l,j+1/2} = \frac{f_{l,j+1} - f_{l,j}}{h_y}, \\ [\nabla_x f]_{i+1/2,m} = \frac{f_{i+3/2,m} - f_{i-1/2,m}}{2h_x}, & [\nabla_y f]_{l,j+1/2} = \frac{f_{l,j+3/2} - f_{l,j-1/2}}{2h_y}, \end{cases}$$

and $\mathbf{D}H = (D_x H, D_y H)$ for any discrete scalar or vector function H . We define the discrete l^2 inner products and norms as follows:

$$\begin{aligned} (f, g)_{l^2,M} &\equiv \sum_{i=0}^{N_x-1} \sum_{j=0}^{N_y-1} h_x h_y f_{i+1/2,j+1/2} g_{i+1/2,j+1/2}, & \|f\|_{l^2,\xi}^2 &\equiv (f, f)_{l^2,\xi}, \\ (f, g)_{l^2,T_x} &\equiv \sum_{i=0}^{N_x} \sum_{j=1}^{N_y-1} h_x h_y f_{i,j} g_{i,j}, & (f, g)_{l^2,T_y} &\equiv \sum_{i=1}^{N_x-1} \sum_{j=0}^{N_y} h_x h_y f_{i,j} g_{i,j}. \end{aligned}$$

We further define discrete l^2 inner products and norms as follows:

$$\begin{aligned} (f, g)_{l^2,T,M} &\equiv \sum_{i=1}^{N_x-1} \sum_{j=0}^{N_y-1} h_x h_y f_{i,j+1/2} g_{i,j+1/2}, & \|f\|_{l^2,T,M}^2 &\equiv (f, f)_{l^2,T,M}, \\ (f, g)_{l^2,M,T} &\equiv \sum_{i=0}^{N_x-1} \sum_{j=1}^{N_y-1} h_x h_y f_{i+1/2,j} g_{i+1/2,j}, & \|f\|_{l^2,M,T}^2 &\equiv (f, f)_{l^2,M,T}. \end{aligned}$$

For vector-valued functions $\mathbf{u} = (u_1, u_2)$, we define

$$\|d_x u_1\|_{l^2,M}^2 \equiv \sum_{i=0}^{N_x-1} \sum_{j=0}^{N_y-1} h_x h_y |d_x u_{1,i+1/2,j+1/2}|^2, \quad \|D_y u_1\|_{l^2,T_y}^2 \equiv \sum_{i=1}^{N_x-1} \sum_{j=0}^{N_y} h_x h_y |D_y u_{1,i,j}|^2,$$

and $\|d_y u_2\|_{l^2,M}$, $\|D_x u_2\|_{l^2,T_x}$ can be defined similarly. Finally, we define the discrete H^1 -norm and the discrete l^2 -norm of a vectored-valued function \mathbf{u} ,

$$\begin{aligned} \|\mathbf{D}\mathbf{u}\|^2 &\equiv \|d_x u_1\|_{l^2,M}^2 + \|D_y u_1\|_{l^2,T_y}^2 + \|D_x u_2\|_{l^2,T_x}^2 + \|d_y u_2\|_{l^2,M}^2, \\ \|\mathbf{u}\|_{l^2}^2 &\equiv \|u_1\|_{l^2,T,M}^2 + \|u_2\|_{l^2,M,T}^2. \end{aligned}$$

Denote $\{\Phi^n, W^n, S^n, \mathbf{U}^n, P^n\}_{n=1}^N$ to be the approximations to $\{\phi^n, \mu^n, s^n, \mathbf{u}^n, p^n\}_{n=1}^N$, respectively, with the boundary conditions

$$\begin{cases} [D_x \Phi]_{0,j+1/2}^n = [D_x \Phi]_{N_x,j+1/2}^n = 0, & 0 \leq j \leq N_y - 1, \\ [D_y \Phi]_{i+1/2,0}^n = [D_y \Phi]_{i+1/2,N_y}^n = 0, & 0 \leq i \leq N_x - 1, \\ \tilde{U}_{1,0,j+1/2}^n = \tilde{U}_{1,N_x,j+1/2}^n = 0, & 0 \leq j \leq N_y - 1, \\ \tilde{U}_{1,i,0}^n = \tilde{U}_{1,i,N_y}^n = 0, & 0 \leq i \leq N_x, \\ \tilde{U}_{2,0,j}^n = \tilde{U}_{2,N_x,j}^n = 0, & 0 \leq j \leq N_y, \\ \tilde{U}_{2,i+1/2,0}^n = \tilde{U}_{2,i+1/2,N_y}^n = 0, & 0 \leq i \leq N_x - 1, \end{cases}$$

and initial conditions

$$\begin{cases} \Phi_{i+1/2,j+1/2}^0 = \phi_{i+1/2,j+1/2}^0, & 0 \leq i \leq N_x - 1, \quad 0 \leq j \leq N_y - 1, \\ \tilde{U}_{1,i,j+1/2}^0 = u_{1,i,j+1/2}^0, & 0 \leq i \leq N_x, \quad 0 \leq j \leq N_y, \\ \tilde{U}_{2,i+1/2,j}^0 = u_{2,i+1/2,j}^0, & 0 \leq i \leq N_x, \quad 0 \leq j \leq N_y, \end{cases}$$

where ϕ^0, \mathbf{u}^0 are given initial conditions.

3 Fully Discrete Generalized sESAV-MBP-Preserving Schemes

In this section, we construct first- and second-order (in time) linear numerical schemes for the nonlocal ACNS model that preserves the energy dissipation law unconditionally and the MBP. For simplicity, we only consider the case that $h = h_x = h_y$, i.e., equal uniform grids are used both in the x and y -directions.

3.1 Semi-Discretized Pressure-Correction Generalized sESAV Scheme

The first-order semi-discretized pressure-correction [8] generalized sESAV scheme is as follows:

Step 1: given (ϕ^n, \mathbf{u}^n) , compute (ϕ^{n+1}, μ^{n+1}) such that

$$\frac{\phi^{n+1} - \phi^n}{\Delta t} + \xi^n \mathbf{u}^n \cdot \nabla \phi^{n+1} = -\mathcal{M} \mu^{n+1}; \quad (3.13a)$$

$$\mu^{n+1} = -\lambda(\epsilon^2 \Delta \phi^{n+1} + \xi^n \bar{f}(\phi^n)) + \kappa \lambda \xi^n (\phi^{n+1} - \phi^n); \quad (3.13b)$$

Step 2: compute $\tilde{\mathbf{u}}^{n+1}$ from

$$\frac{\tilde{\mathbf{u}}^{n+1} - \mathbf{u}^n}{\Delta t} + \xi^n (\mathbf{u}^n \cdot \nabla) \mathbf{u}^n - \nu \Delta \tilde{\mathbf{u}}^{n+1} + \nabla p^n = \mu^{n+1} \nabla \phi^{n+1}, \quad \tilde{\mathbf{u}}^{n+1}|_{\partial\Omega} = 0; \quad (3.13c)$$

Step 3: update \mathbf{u}^{n+1} using

$$\frac{\mathbf{u}^{n+1} - \tilde{\mathbf{u}}^{n+1}}{\Delta t} + \nabla(p^{n+1} - p^n) = 0; \quad \nabla \cdot \mathbf{u}^{n+1} = 0, \quad \mathbf{u}^{n+1} \cdot \mathbf{n}|_{\partial\Omega} = 0; \quad (3.13d)$$

Step 4: solve s^{n+1} from

$$\begin{aligned} \frac{\tilde{s}^{n+1} - s^n}{\Delta t} &= \int_{\Omega} -\mu^{n+1} \nabla \phi^{n+1} \cdot \tilde{\mathbf{u}}^{n+1} \\ &\quad - \xi^n \left(\lambda \bar{f}(\phi^n) \frac{\phi^{n+1} - \phi^n}{\Delta t} - \gamma \mathbf{u}^n \cdot \nabla \mathbf{u}^n \cdot \tilde{\mathbf{u}}^{n+1} - \nabla \cdot (\mathbf{u}^n \phi^{n+1}) \mu^{n+1} \right) dx; \\ s^{n+1} &= \max \{ \tilde{s}^{n+1}, -C_* - E_{el}[\phi^{n+1}, \mathbf{u}^{n+1}, p^{n+1}] \}, \end{aligned} \quad (3.13e)$$

where

$$\xi^n = \frac{\sigma(s^n)}{\sigma(E_1(\phi^n))},$$

and

$$E_{el}[\phi^{n+1}, \mathbf{u}^{n+1}, p^{n+1}] = \frac{\lambda \epsilon^2}{2} \|\nabla \phi^{n+1}\|^2 + \frac{1}{2} \|\mathbf{u}^{n+1}\|^2 + \frac{\Delta t^2}{2} \|\nabla p^{n+1}\|^2.$$

The second-order semi-discretized pressure-correction generalized sESAV scheme is as follows:

Step 1: given $(\phi^n, \phi^{n-1}, \mathbf{u}^n, \mathbf{u}^{n-1})$, compute (ϕ^{n+1}, μ^{n+1}) such that

$$\frac{\phi^{n+1} - \phi^n}{\Delta t} + \xi^{*,n+1/2} \mathbf{u}^{*,n+1/2} \cdot \nabla \phi^{n+1/2} = -\mathcal{M} \mu^{n+1/2}, \quad (3.14a)$$

$$\begin{aligned} \mu^{n+1/2} = & -\lambda \epsilon^2 \Delta \phi^{n+1/2} - \lambda \xi^{*,n+1/2} \bar{f}(\phi^{*,n+1/2}) \\ & + \kappa \lambda \xi^{*,n+1/2} (\phi^{n+1/2} - \phi^{*,n+1/2}); \end{aligned} \quad (3.14b)$$

Step 2: solve $\tilde{\mathbf{u}}^{n+1}$ from

$$\begin{aligned} \frac{\tilde{\mathbf{u}}^{n+1} - \mathbf{u}^n}{\Delta t} + \xi^{*,n+1/2} (\mathbf{u}^{*,n+1/2} \cdot \nabla) \mathbf{u}^{*,n+1/2} - \nu \Delta \frac{\tilde{\mathbf{u}}^{n+1} + \mathbf{u}^n}{2} \\ + \nabla p^n = \mu^{n+1/2} \nabla \phi^{n+1/2}, \quad \tilde{\mathbf{u}}^{n+1}|_{\partial\Omega} = 0; \end{aligned} \quad (3.14c)$$

Step 3: update \mathbf{u}^{n+1} using

$$\begin{aligned} \frac{\mathbf{u}^{n+1} - \tilde{\mathbf{u}}^{n+1}}{\Delta t} + \frac{1}{2} \nabla (p^{n+1} - p^n) = 0, \\ \nabla \cdot \mathbf{u}^{n+1} = 0, \quad \mathbf{u}^{n+1} \cdot \mathbf{n}|_{\partial\Omega} = 0; \end{aligned} \quad (3.14d)$$

Step 4: solve s^{n+1} from

$$\begin{aligned} \frac{\tilde{s}^{n+1} - s^n}{\Delta t} = & \int_{\Omega} -\mu^{n+1/2} \nabla \phi^{n+1/2} \cdot \frac{\tilde{\mathbf{u}}^{n+1} + \mathbf{u}^n}{2} - \lambda \xi^{*,n+1/2} \bar{f}(\phi^{*,n+1/2}) \frac{\phi^{n+1} - \phi^n}{\Delta t} \\ & + \xi^{*,n+1/2} \left(\gamma \mathbf{u}^{*,n+1/2} \cdot \nabla \mathbf{u}^{*,n+1/2} \cdot \frac{\tilde{\mathbf{u}}^{n+1} + \mathbf{u}^n}{2} + \nabla \cdot (\mathbf{u}^{*,n+1/2} \phi^{n+1/2}) \mu^{n+1/2} \right) \\ & + \kappa \xi^{*,n+1/2} (\phi^{n+1/2} - \phi^{*,n+1/2}) \cdot \frac{\phi^{n+1} - \phi^n}{\Delta t} d\mathbf{x}, \\ s^{n+1} = & \max \{ \tilde{s}^{n+1}, -C_* - E_{el}[\phi^{n+1}, \mathbf{u}^{n+1}, p^{n+1}] \}, \end{aligned} \quad (3.14e)$$

where

$$\xi^{*,n+1/2} = \frac{\sigma(s^{*,n+1/2})}{\sigma(E_1(\phi^{*,n+1/2}))},$$

and

$$E_{el}[\phi^{n+1}, \mathbf{u}^{n+1}, p^{n+1}] = \frac{\lambda \epsilon^2}{2} \|\nabla \phi^{n+1}\|^2 + \frac{1}{2} \|\mathbf{u}^{n+1}\|^2 + \frac{\Delta t^2}{8} \|\nabla p^{n+1}\|^2.$$

$(\cdot)^{n+1/2} = \frac{1}{2}(\cdot)^{n+1} + \frac{1}{2}(\cdot)^n$ and $(\cdot)^{*,n+1/2}$ are generated by the first-order scheme (3.13) with the time step size $\Delta t/2$.

3.2 Fully Discrete MBP-sESAV Scheme with First-Order in Time

Scheme 1 (MBP-sESAV1 scheme) Based on the MAC discretization, the fully discrete first-order pressure-correction generalized sESAV scheme is given as follows:

Step 1: given (Φ^n, \mathbf{U}^n) , compute (Φ^{n+1}, W^{n+1}) such that

$$\frac{\Phi^{n+1} - \Phi^n}{\Delta t} + \chi^n (\Pi_h(U_1^n) \nabla_x + \Pi_h(U_2^n) \nabla_y) \Phi^{n+1} = -\mathcal{M} W^{n+1}, \quad (3.15a)$$

$$\begin{aligned} W^{n+1} &= -\lambda\epsilon^2 [d_x D_x \Phi + d_y D_y \Phi]^{n+1} - \lambda \chi^n \bar{f}(\Phi^n) \\ &\quad + \kappa \lambda \chi^n (\Phi^{n+1} - \Phi^n); \end{aligned} \quad (3.15b)$$

Step 2: solve \tilde{U}^{n+1} from

$$\begin{aligned} \frac{\tilde{U}_1^{n+1} - U_1^n}{\Delta t} + \chi^n C_1^n - \nu D_x (d_x \tilde{U}_1)^{n+1} - \nu d_y (D_y \tilde{U}_1)^{n+1} \\ + [D_x P]^n = \Pi_h W^{n+1} [D_x \Phi]^{n+1}, \quad \tilde{U}_1^{n+1}|_{\partial\Omega} = 0, \end{aligned} \quad (3.15c)$$

$$\begin{aligned} \frac{\tilde{U}_2^{n+1} - U_2^n}{\Delta t} + \chi^n C_2^n - \nu D_y (d_y \tilde{U}_2)^{n+1} - \nu d_x (D_x \tilde{U}_2)^{n+1}, \\ + [D_y P]^n = \Pi_h W^{n+1} [D_y \Phi]^{n+1}, \quad \tilde{U}_2^{n+1}|_{\partial\Omega} = 0; \end{aligned} \quad (3.15d)$$

Step 3: given (\tilde{U}^{n+1}, P^n) , find (U^{n+1}, P^{n+1}) by solving

$$\frac{U_1^{n+1} - \tilde{U}_1^{n+1}}{\Delta t} + ([D_x P]^{n+1} - [D_x P]^n) = 0, \quad (3.15e)$$

$$\frac{U_2^{n+1} - \tilde{U}_2^{n+1}}{\Delta t} + ([D_y P]^{n+1} - [D_y P]^n) = 0, \quad (3.15f)$$

$$[d_x U_1]^{n+1} + [d_y U_2]^{n+1} = 0, \quad \mathbf{U}^{n+1} \cdot \mathbf{n}|_{\partial\Omega} = 0; \quad (3.15g)$$

By taking the operator dx of (3.15e) and the operator dy of (3.15f), we find that (3.15g) is equivalent to

$$(d_x D_x + d_y D_y)(P^{n+1} - P^n) = \frac{1}{\Delta t} (d_x \tilde{U}_1^{n+1} + d_y \tilde{U}_2^{n+1}), \quad \mathbf{D}(P^{n+1} - P^n) \cdot \mathbf{n}|_{\partial\Omega} = 0, \quad (3.15h)$$

$$U_1^{n+1} = \tilde{U}_1^{n+1} - \Delta t ([D_x P]^{n+1} - [D_x P]^n), \quad (3.15i)$$

$$U_2^{n+1} = \tilde{U}_2^{n+1} - \Delta t ([D_y P]^{n+1} - [D_y P]^n); \quad (3.15j)$$

Step 4: solve S^{n+1} from

$$\begin{aligned} \frac{\tilde{S}^{n+1} - S^n}{\Delta t} &= - \left(\Pi_h W^{n+1} D_x \Phi^{n+1}, \tilde{U}_1^{n+1} \right)_{l^2, T, M} - \left(\Pi_h W^{n+1} D_y \Phi^{n+1}, \tilde{U}_2^{n+1} \right)_{l^2, M, T} \\ &\quad - \lambda \chi^n \left(\bar{f}(\Phi^n), \frac{\Phi^{n+1} - \Phi^n}{\Delta t} \right)_{l^2, M} + \gamma \chi^n (C_1^n, \tilde{U}_1^{n+1})_{l^2, T, M} \\ &\quad + \gamma \chi^n (C_2^n, \tilde{U}_2^{n+1})_{l^2, M, T} + \chi^n (\Pi_h (U_1^n) \bar{d}_x \Phi^{n+1} + \Pi_h (U_2^n) \bar{d}_y \Phi^{n+1}, W^{n+1})_{l^2, M}, \end{aligned} \quad (3.15k)$$

$$S^{n+1} = \max \left\{ \tilde{S}^{n+1}, -C_* - E_{el}^{n+1}[\Phi, \mathbf{U}, P] \right\},$$

where Π_h is the bilinear interpolation operator and

$$\chi^n = \frac{\sigma(S^n)}{\sigma(E_1^h(\Phi^n))},$$

$$C_1^n = [U_1 D_x (\Pi_h U_1) + \Pi_h U_2 d_y (\Pi_h U_1)]^n,$$

$$C_2^n = [\Pi_h U_1 d_x (\Pi_h U_2) + U_2 D_y (\Pi_h U_2)]^n,$$

$$E_{el}^{n+1}[\Phi, \mathbf{U}, P] = \frac{\lambda\epsilon^2}{2} \|\mathbf{D}\Phi^{n+1}\|^2 + \frac{1}{2} \|\mathbf{U}^{n+1}\|^2 + \frac{\Delta t^2}{2} \|\mathbf{D}P^{n+1}\|^2.$$

Remark 3.1 We only need to calculate two linear elliptic equations in Step 2, and two Poisson-type equations in Step 3, which leads to extremely efficient calculations. Finally, we can determine S^{n+1} by solving a linear algebraic equation with negligible computational cost.

Lemma 3.1 ([33]) *Let $\{V_{1,i,j+1/2}\}, \{V_{2,i+1/2,j}\}, \{q_{1,i+1/2,j+1/2}\}, \{q_{2,i+1/2,j+1/2}\}$ be discrete functions with $V_{1,0,j+1/2} = V_{1,N_x,j+1/2} = V_{2,i+1/2,0} = V_{2,i+1/2,N_y} = 0$ for proper integers i and j . Then, there holds*

$$(D_x q_1, V_1)_{l^2,T,M} = -(q_1, d_x V_1)_{l^2,M}, \quad (D_y q_2, V_2)_{l^2,M,T} = -(q_2, d_y V_2)_{l^2,M}.$$

We proceed to prove the unconditional energy dissipation and MBP of the scheme defined in (3.13) as follows.

Theorem 3.1 (Energy stable of the MBP-sESAVI scheme) *The scheme (3.15) is energy stable in the sense that*

$$E_h^{n+1}(\Phi, U, S) - E_h^n(\Phi, U, S) \leq -M\Delta t \|W^{n+1}\|_{l^2,M}^2 - \nu\Delta t \|D\tilde{U}^{n+1}\|^2, \quad (3.16)$$

where

$$E_h^{n+1}(\Phi, U, S) = \frac{\lambda\epsilon^2}{2} \|\mathbf{D}\Phi^{n+1}\|_{l^2}^2 + \frac{1}{2} \|\mathbf{U}^{n+1}\|_{l^2}^2 + \frac{\Delta t^2}{2} \|\mathbf{D}P^{n+1}\|_{l^2}^2 + S^{n+1}.$$

Proof Multiplying (3.15a) with $W_{i+1/2,j+1/2}^{n+1} h_x h_y$ and taking summation over i, j for $0 \leq i \leq N_x - 1, 0 \leq j \leq N_y - 1$, we have

$$\begin{aligned} & \left(\frac{\Phi^{n+1} - \Phi^n}{\Delta t}, W^{n+1} \right)_{l^2,M} + \chi^n \left((\Pi_h(U_1^n) \nabla_x + \Pi_h(U_2^n) \nabla_y) \Phi^{n+1}, W^{n+1} \right)_{l^2,M} \\ & = -\mathcal{M} \|W^{n+1}\|_{l^2,M}^2. \end{aligned} \quad (3.17)$$

Multiplying (3.15b) with $\frac{(\Phi^{n+1} - \Phi^n)_{i+1/2,j+1/2}}{\Delta t} h_x h_y$ and taking summation over i, j for $0 \leq i \leq N_x - 1, 0 \leq j \leq N_y - 1$, we have

$$\begin{aligned} \left(\frac{\Phi^{n+1} - \Phi^n}{\Delta t}, W^{n+1} \right)_{l^2,M} &= -\lambda\epsilon^2 (d_x D_x \Phi^{n+1} + d_y D_y \Phi^{n+1}, \frac{\Phi^{n+1} - \Phi^n}{\Delta t})_{l^2,M} \\ &\quad - \lambda\chi^n \left(\bar{f}(\Phi^n), \frac{\Phi^{n+1} - \Phi^n}{\Delta t} \right)_{l^2,M} + \frac{\kappa\lambda\chi^n}{\Delta t} \|\Phi^{n+1} - \Phi^n\|_{l^2,M}^2. \end{aligned} \quad (3.18)$$

Using Lemma 3.1, the first term on the right-hand side of (3.18) can be estimated by

$$\begin{aligned} & - (d_x D_x \Phi^{n+1} + d_y D_y \Phi^{n+1}, \frac{\Phi^{n+1} - \Phi^n}{\Delta t})_{l^2,M} \\ &= (D_x \Phi^{n+1}, \frac{D_x \Phi^{n+1} - D_x \Phi^n}{\Delta t})_{l^2,T,M} \\ &+ (D_y \Phi^{n+1}, \frac{D_y \Phi^{n+1} - D_y \Phi^n}{\Delta t})_{l^2,M,T} \geq \frac{\|\mathbf{D}\Phi^{n+1}\|_{l^2}^2 - \|\mathbf{D}\Phi^n\|_{l^2}^2}{2\Delta t}. \end{aligned} \quad (3.19)$$

Multiplying (3.15c) by $\tilde{U}_{1,i,j+1/2}^{n+1} h_x h_y$, and taking summation over i, j for $1 \leq i \leq N_x - 1$, $0 \leq j \leq N_y - 1$ yields

$$\begin{aligned} & \left(\frac{\tilde{U}_1^{n+1} - U_1^n}{\Delta t}, \tilde{U}_1^{n+1} \right)_{l^2, T, M} + \chi^n (C_1^n, \tilde{U}_1^{n+1})_{l^2, T, M} \\ & + \nu \|d_x \tilde{U}_1^{n+1}\|_{l^2, M} + \nu \|D_y \tilde{U}_1^{n+1}\|_{l^2, T_y} \\ & - (P^n, d_x \tilde{U}_1^{n+1})_{l^2, M} - (\Pi_h W^{n+1} D_x \Phi^{n+1}, \tilde{U}_1^{n+1})_{l^2, T, M} = 0. \end{aligned} \quad (3.20)$$

Multiplying (3.15d) by $\tilde{U}_{2,i+1/2,j}^{n+1} h_x h_y$, and taking summation over i, j for $0 \leq i \leq N_x - 1$, $1 \leq j \leq N_y - 1$ leads to

$$\begin{aligned} & \left(\frac{\tilde{U}_2^{n+1} - U_2^n}{\Delta t}, \tilde{U}_2^{n+1} \right)_{l^2, M, T} + \chi^n (C_2^n, \tilde{U}_2^{n+1})_{l^2, M, T} \\ & + \nu \|d_x \tilde{U}_2^{n+1}\|_{l^2, M} + \nu \|D_x \tilde{U}_2^{n+1}\|_{l^2, T_x} \\ & - (P^n, d_y \tilde{U}_2^{n+1})_{l^2, M} - (\Pi_h W^{n+1} D_y \Phi^{n+1}, \tilde{U}_2^{n+1})_{l^2, M, T} = 0. \end{aligned} \quad (3.21)$$

Next, we rewrite (3.15e)-(3.15f) as

$$\begin{aligned} \frac{U_1^{n+1}}{\sqrt{\Delta t}} + \sqrt{\Delta t} D_x P^{n+1} &= \frac{\tilde{U}_1^{n+1}}{\sqrt{\Delta t}} + \sqrt{\Delta t} D_x P^n, \\ \frac{U_2^{n+1}}{\sqrt{\Delta t}} + \sqrt{\Delta t} D_y P^{n+1} &= \frac{\tilde{U}_2^{n+1}}{\sqrt{\Delta t}} + \sqrt{\Delta t} D_y P^n, \end{aligned}$$

now taking the discrete inner product with themselves on both sides and summing them up, it is clear that we have

$$\begin{aligned} \frac{1}{\Delta t} \|U^{n+1}\|_{l^2}^2 + \Delta t \|\mathbf{D}P^{n+1}\|_{l^2}^2 &= \frac{1}{\Delta t} \|\tilde{U}^{n+1}\|_{l^2}^2 + \Delta t \|\mathbf{D}P^n\|_{l^2}^2 \\ &\quad - 2(P^n, d_x \tilde{U}_1^{n+1})_{l^2, M} - 2(P^n, d_y \tilde{U}_2^{n+1})_{l^2, M}. \end{aligned} \quad (3.22)$$

Combining (3.17)-(3.21) with (3.22), (3.15k) and (3.15g), we obtain

$$E_h^{n+1}(\Phi, U, \tilde{S}) - E_h^n(\Phi, U, S) \leq 0.$$

If $\tilde{s}^{n+1} \geq -C_* - E_{el}^{n+1}[\Phi, \mathbf{U}, P]$, it follows that $S^{n+1} = \tilde{S}^{n+1}$, and, consequently,

$$E_h^{n+1}(\Phi, U, S) - E_h^n(\Phi, U, S) \leq 0. \quad (3.23)$$

In the case where $\tilde{S}^{n+1} < -C_* - E_{el}^{n+1}[\Phi, \mathbf{U}, P]$, we observe that

$$S^{n+1} + E_{el}^{n+1}[\Phi, \mathbf{U}, P] = -C_* \leq S^n + E_{el}^n[\Phi, \mathbf{U}, P],$$

leading directly to (3.16). \square

Corollary 3.1 *It holds $S^n \leq \mathcal{E}_h[\Phi_{\text{init}}, \mathbf{U}_{\text{init}}]$ for any $\kappa \geq 0$.*

Proof By Theorem 3.1, and since $S_0 = E_{1h}(\Phi_{\text{init}})$, we have

$$\begin{aligned} & \int_{\Omega} \frac{\lambda \epsilon^2}{2} |\mathbf{D}\Phi^n|^2 + \frac{1}{2} |\mathbf{U}^n|^2 + \frac{\Delta t^2}{2} |\mathbf{D}P^n|^2 d\mathbf{x} + S^n \\ & = E_h^n[\Phi, \mathbf{U}, S] \leq E_h^{n-1}[\Phi, \mathbf{U}, S] \leq \dots \leq E_h^0[\Phi, \mathbf{U}, S] = \mathcal{E}_h[\Phi_{\text{init}}, \mathbf{U}_{\text{init}}], \end{aligned} \quad (3.24)$$

dropping off the nonnegative term, we can easily obtain the desired result. \square

Remark 3.2 Employing a similar error analysis as in [34], one can conclude that:

$$\|\mathbf{u}(t^n) - \mathbf{U}^n\|_{L^2} \leq \bar{C}(h^2 + \Delta t).$$

Noting the inverse inequality, we derive

$$\begin{aligned} \|\mathbf{U}^n\|_{L^\infty} &\leq \|\mathbf{U}^n - \Pi_h \mathbf{u}\|_{L^\infty} + \|\Pi_h \mathbf{u} - \mathbf{u}(t^n)\|_{L^\infty} + \|\mathbf{u}(t^n)\|_{L^\infty} \\ &\leq \bar{C}h^{-\frac{d}{2}} (\|\mathbf{U}^n - \mathbf{u}(t^n)\|_{L^2} + \|\Pi_h \mathbf{u} - \mathbf{u}(t^n)\|_{L^2}) + \|\Pi_h \mathbf{u} - \mathbf{u}(t^n)\|_{L^\infty} + \|\mathbf{u}(t^n)\|_{L^\infty} \\ &\leq \bar{C}h^{-\frac{d}{2}} (h^2 + \Delta t) + \|\Pi_h \mathbf{u} - \mathbf{u}(t^n)\|_{L^\infty} + \|\mathbf{u}(t^n)\|_{L^\infty} \leq \hat{C}, \end{aligned}$$

with the following estimation $\|\Pi_h \mathbf{u} - \mathbf{u}\|_{L^\infty} \leq \bar{C}h^2$.

Theorem 3.2 (Discrete MBP of the MBP-sESAVI scheme) *Let f be continuously differentiable on $[-\beta, \beta]$ such that $\kappa \geq \|f'\|_{C[-\beta, \beta]}$. Moreover, if h satisfy*

$$h \leq \frac{2\lambda\epsilon^2\mathcal{M}}{\hat{C}G^*},$$

where $\hat{C} > 0$ is defined in Remark 3.2 and $G^* = \exp\{\mathcal{E}_h(\Phi_{init}, \mathbf{U}_{init}) + C_*\}$, then the scheme preserves the MBP unconditionally, i.e.,

$$\|\Phi_{init}\|_{L^\infty(\Omega)} \leq \beta \Rightarrow \|\Phi^n\|_{L^\infty(\Omega)} \leq \beta, \quad \forall n.$$

Proof We prove the statement by induction. Suppose (Φ^n, S^n) is given and $\|\Phi^n\|_{L^\infty(\Omega)} \leq \beta$ for some n . Notice that $\chi^n(\Phi, S) > 0$ from its definition. It is obvious that using Corollary 3.1, we can get $\chi^n(\Phi, S) \leq \exp\{\mathcal{E}_h(\Phi_{init}, \mathbf{U}_{init}) + C_*\} = G^*(\Phi_{init}, \mathbf{U}_{init}, C_*)$.

We eliminate Φ^{n+1} from (3.15a)-(3.15b) to get

$$\left(\left(\frac{1}{\Delta t} + \mathcal{M}\lambda\kappa\chi^n \right) I - \mathcal{L}_{\mathbf{U}^n} \right) \Phi^{n+1} = \frac{1}{\Delta t} \Phi^n + \mathcal{M}\lambda\chi^n (\bar{f}(\Phi^n) + \kappa\Phi^n),$$

where

$$\mathcal{L}_{\mathbf{U}^n} = \mathcal{M}\lambda\epsilon^2(d_x D_x + d_y D_y) - \chi^n (\Pi_h(U_1^n) \nabla_x + \Pi_h(U_2^n) \nabla_y).$$

Without loss of generality, we shall describe the specific discrete scheme of $\mathcal{L}_{\mathbf{U}^n}$ for one-dimensional systems, the extensions to two-dimensional and three-dimensional rectangular domains are straightforward.

$$\mathcal{L}_{\mathbf{U}^n} = \begin{bmatrix} -w + \frac{\chi^n |\Pi_h U_{1/2}|}{2h} & w - \frac{\chi^n |\Pi_h U_{1/2}|}{2h} & & & \\ w + \frac{\chi^n |\Pi_h U_{3/2}|}{2h} & -2w & w - \frac{\chi^n |\Pi_h U_{3/2}|}{2h} & & \\ & \ddots & \ddots & \ddots & \\ & w + \frac{\chi^n |\Pi_h U_{N-3/2}|}{2h} & -2w & w - \frac{\chi^n |\Pi_h U_{N-3/2}|}{2h} & \\ & & w + \frac{\chi^n |\Pi_h U_{N-1/2}|}{2h} & -w - \frac{\chi^n |\Pi_h U_{N-1/2}|}{2h} & \end{bmatrix},$$

where $w = \frac{\mathcal{M}\lambda\epsilon^2}{h^2}$. Due to $0 < \chi^n \leq G^*$, the condition

$$h \max \left\{ \left\| \Pi_h U_{1,i,j}^n \right\|_{L^\infty}, \left\| \Pi_h U_{2,i,j}^n \right\|_{L^\infty} \right\} \leq h\hat{C} \leq \frac{2\lambda\epsilon^2\mathcal{M}}{G^*},$$

can be guaranteed holds, then all off-diagonal entries of $\mathcal{L}_{\mathbf{U}^n}$ are non-positive and diagonal entries of $\mathcal{L}_{\mathbf{U}^n}$ are positive, thus $\mathcal{L}_{\mathbf{U}^n}$ is a negative diagonally dominant matrix by rows. We can easily demonstrate that the coefficient matrix of (3.15a)-(3.15b) satisfies Lemma 2.1.

Then by Lemma 2.1, we can have

$$\left\| \left(\left(\frac{1}{\Delta t} + \mathcal{M}\kappa\lambda\chi^n \right) I - \mathcal{L}_{\mathbf{U}^n} \right)^{-1} \right\|_{L^\infty(\Omega)} \leq \left(\frac{1}{\Delta t} + \mathcal{M}\kappa\lambda\chi^n \right)^{-1}.$$

According to Lemma 2.2, we derive

$$\left\| \frac{1}{\Delta t} \Phi^n + \mathcal{M}\lambda\chi^n (\bar{f}(\Phi^n) + \kappa\Phi^n) \right\|_{L^\infty(\Omega)} \leq \left(\frac{1}{\Delta t} + \mathcal{M}\kappa\lambda\chi^n \right) \beta.$$

Therefore, we finally obtain

$$\|\Phi^{n+1}\|_{L^\infty(\Omega)} \leq \left(\frac{1}{\Delta t} + \mathcal{M}\kappa\lambda\chi^n \right)^{-1} \left(\frac{1}{\Delta t} + \mathcal{M}\kappa\lambda\chi^n \right) \beta = \beta.$$

Since $\|\Phi_{\text{init}}\|_{L^\infty(\Omega)} \leq \beta$, by induction $\|\Phi^n\|_{L^\infty(\Omega)} \leq \beta$ for all n . \square

3.3 Fully Discrete MBP-sESAV Scheme with Second-Order in Time

Scheme 2 (MBP-sESAV2 scheme) *The fully discrete second-order pressure-correction generalized sESAV scheme based on the MAC discretization is as follows:*

Step 1: given $(\Phi^n, \Phi^{n-1}, \mathbf{U}^n, \mathbf{U}^{n-1})$, compute (Φ^{n+1}, W^{n+1}) such that

$$\frac{\Phi^{n+1} - \Phi^n}{\Delta t} + \chi^{*,n+1/2} \left(\Pi_h \left(U_1^{*,n+1/2} \right) \nabla_x + \Pi_h \left(U_2^{*,n+1/2} \right) \nabla_y \right) \Phi^{n+1/2} = -\mathcal{M}W^{n+1/2}, \quad (3.25a)$$

$$\begin{aligned} W^{n+1/2} = & -\lambda\epsilon^2 [d_x D_x \Phi + d_y D_y \Phi]^{n+1/2} - \lambda\chi^{*,n+1/2} \bar{f}(\Phi^{*,n+1/2}) \\ & + \kappa\lambda\chi^{*,n+1/2} (\Phi^{n+1/2} - \Phi^{*,n+1/2}); \end{aligned} \quad (3.25b)$$

Step 2: solve for $\tilde{\mathbf{U}}^{n+1}$ from

$$\begin{aligned} \frac{\tilde{U}_1^{n+1} - U_1^n}{\Delta t} - \nu D_x \left(\frac{d_x \tilde{U}_1^{n+1} + d_x U_1^n}{2} \right) - \nu d_y \left(\frac{D_y \tilde{U}_1^{n+1} + D_y U_1^n}{2} \right) \\ + \chi^{*,n+1/2} C_1^{*,n+1/2} + [D_x P]^n - \Pi_h W^{n+1/2} [D_x \Phi]^{n+1/2} = 0, \quad \tilde{U}_1^{n+1}|_{\partial\Omega} = 0, \end{aligned} \quad (3.25c)$$

$$\begin{aligned} \frac{\tilde{U}_2^{n+1} - U_2^n}{\Delta t} - \nu D_y \left(\frac{d_y \tilde{U}_2^{n+1} + d_y U_2^n}{2} \right) - \nu d_x \left(\frac{D_x \tilde{U}_2^{n+1} + D_x U_2^n}{2} \right) \\ + \chi^{*,n+1/2} C_2^{*,n+1/2} + [D_y P]^n - \Pi_h W^{n+1/2} [D_y \Phi]^{n+1/2} = 0, \quad \tilde{U}_2^{n+1}|_{\partial\Omega} = 0; \end{aligned} \quad (3.25d)$$

Step 3: given $(\tilde{\mathbf{U}}^{n+1}, P^n)$, find $(\mathbf{U}^{n+1}, P^{n+1})$ by solving

$$\frac{U_1^{n+1} - \tilde{U}_1^{n+1}}{\Delta t} + \frac{1}{2} (D_x P^{n+1} - D_x P^n) = 0, \quad (3.25e)$$

$$\frac{U_2^{n+1} - \tilde{U}_2^{n+1}}{\Delta t} + \frac{1}{2} (D_y P^{n+1} - D_y P^n) = 0, \quad (3.25f)$$

$$[d_x U_1]^{n+1} + [d_y U_2]^{n+1} = 0, \quad \mathbf{U}^{n+1} \cdot \mathbf{n}|_{\partial\Omega} = 0; \quad (3.25g)$$

Similar procedures for solving (3.25e)-(3.25g) are discussed in (3.15h)-(3.15j) as follows. By taking the operator dx of (3.25e) and the operator dy of (3.25f), we find that (3.25g) is equivalent to

$$(d_x D_x + d_y D_y)(P^{n+1} - P^n) = \frac{2}{\Delta t}(d_x \tilde{U}_1^{n+1} + d_y \tilde{U}_2^{n+1}), \quad \mathbf{D}(P^{n+1} - P^n) \cdot \mathbf{n}|_{\partial\Omega} = 0, \quad (3.25h)$$

$$U_1^{n+1} = \tilde{U}_1^{n+1} - \frac{\Delta t}{2}([D_x P]^{n+1} - [D_x P]^n), \quad (3.25i)$$

$$U_2^{n+1} = \tilde{U}_2^{n+1} - \frac{\Delta t}{2}([D_y P]^{n+1} - [D_y P]^n); \quad (3.25j)$$

Step 4: solve for S^{n+1} from

$$\begin{aligned} \frac{\tilde{S}^{n+1} - S^n}{\Delta t} = & - \left(\Pi_h W^{n+1/2} D_x \Phi^{n+1/2}, \frac{\tilde{U}_1^{n+1} + U_1^n}{2} \right)_{l^2, T, M} \\ & - \left(\Pi_h W^{n+1/2} D_y \Phi^{n+1/2}, \frac{\tilde{U}_2^{n+1} + U_2^n}{2} \right)_{l^2, M, T} \\ & - \lambda \chi^{*, n+1/2} \left(\bar{f}(\Phi^{*, n+1/2}), \frac{\Phi^{n+1} - \Phi^n}{\Delta t} \right)_{l^2, M} \\ & + \gamma \chi^{*, n+1/2} \left(C_1^{*, n+1/2}, \frac{\tilde{U}_1^{n+1} + U_1^n}{2} \right)_{l^2, T, M} + \gamma \chi^{*, n+1/2} \left(C_2^{*, n+1/2}, \frac{\tilde{U}_2^{n+1} + U_2^n}{2} \right)_{l^2, M, T} \\ & + \chi^{*, n+1/2} \left(\left(\Pi_h (U_1^{*, n+1/2}) \nabla_x + \Pi_h (U_2^{*, n+1/2}) \nabla_y \right) \Phi^{n+1/2}, W^{n+1/2} \right)_{l^2, M} \\ & + \kappa \chi^{*, n+1/2} \left(\Phi^{n+1/2} - \Phi^{*, n+1/2}, \frac{\Phi^{n+1} - \Phi^n}{\Delta t} \right)_{l^2, M}, \\ S^{n+1} = & \max \left\{ \tilde{S}^{n+1}, -C_* - E_{el}^{n+1}[\Phi, \mathbf{U}, P] \right\}, \end{aligned} \quad (3.25k)$$

where

$$\begin{aligned} \chi^{*, n+1/2} &= \frac{\sigma(S^{*, n+1/2})}{\sigma(E_1^h(\Phi^{*, n+1/2}))}, \\ C_1^{*, n+1/2} &= [U_1 D_x (\Pi_h U_1) + \Pi_h U_2 d_y (\Pi_h U_1)]^{*, n+1/2}, \\ C_2^{*, n+1/2} &= [\Pi_h U_1 d_x (\Pi_h U_2) + U_2 D_y (\Pi_h U_2)]^{*, n+1/2}, \\ E_{el}^{n+1}[\Phi, \mathbf{U}, P] &= \frac{\lambda \epsilon^2}{2} \|\mathbf{D}\Phi^{n+1}\|^2 + \frac{1}{2} \|\mathbf{U}^{n+1}\|^2 + \frac{\Delta t^2}{8} \|\mathbf{D}P^{n+1}\|^2. \end{aligned}$$

and for any sequence of $\{F^{*, n+1/2}\}$ is generated by the pressure-correction sESAVI scheme (3.15) with the time step size $\Delta t/2$.

Remark 3.3 The computations of $(\mathbf{U}^{n+1}, P^{n+1})$ are decoupled through a second-order pressure correction scheme [35]. The projection method used here has been analyzed in [36], demonstrating that the scheme achieves second-order accuracy for velocity in $l^2(0, T; L^2(\Omega))$, while it is only first-order accurate for pressure in $l^\infty(0, T; L^2(\Omega))$. The loss of accuracy for pressure is due to the artificial boundary condition (3.25e)-(3.25f) imposed on pressure [37]. Additionally, we can achieve 1.5 order accuracy for the pressure by using

the rotational pressure-correction method [38] based on the Backward difference formula (BDF2) discretization. And the Crank-Nicolson scheme with linear extrapolation is widely regarded as a popular time discretization method for the Navier–Stokes equations. We refer to [36, 38–40] and references therein for analysis on this type of discretization.

Next, we prove the unconditional energy stable and MBP of scheme (3.25).

Theorem 3.3 (Energy stable of the MBP-sESAV2 scheme) *The scheme (3.25) is energy stable in the sense that*

$$E_h^{n+1}(\Phi, U, S) - E_h^n(\Phi, U, S) \leq -M\Delta t \|W^{n+1/2}\|_{l^2, M}^2 - \nu\Delta t \left\| \frac{D\tilde{U}^{n+1} + DU^n}{2} \right\|^2, \quad (3.26)$$

where $\mathbf{D}H = (D_x H, D_y H)$ for any discrete scalar or vector function H , and

$$E_h^{n+1}(\Phi, U, S) = \frac{\lambda\epsilon^2}{2} \|\mathbf{D}\Phi^{n+1}\|_{l^2}^2 + \frac{1}{2} \|U^{n+1}\|_{l^2}^2 + \frac{\Delta t^2}{8} \|\mathbf{D}P^{n+1}\|_{l^2}^2 + S^{n+1}.$$

Furthermore, it is ensured that $S^n \leq \mathcal{E}_h[\Phi_{init}, U_{init}]$ and $S^{*,n+1/2} \leq \mathcal{E}_h[\Phi_{init}, U_{init}]$.

Proof Multiplying (3.25a) by $W_{i+1/2, j+1/2}^{n+1/2} h_x h_y$ and taking summation over i, j for $0 \leq i \leq N_x - 1, 0 \leq j \leq N_y - 1$ yields

$$\begin{aligned} & \left(\frac{\Phi^{n+1} - \Phi^n}{\Delta t}, W^{n+1/2} \right)_{l^2, M} \\ & + \chi^{*,n+1/2} \left(\left(\Pi_h \left(U_1^{*,n+1/2} \right) \nabla_x + \Pi_h \left(U_2^{*,n+1/2} \right) \nabla_y \right) \Phi^{n+1/2}, W^{n+1/2} \right)_{l^2, M} \\ & = -\mathcal{M} \|W^{n+1/2}\|_{l^2}^2. \end{aligned} \quad (3.27)$$

Multiplying (3.25b) by $\frac{(\Phi^{n+1} - \Phi^n)_{i+1/2, j+1/2}}{\Delta t} h_x h_y$ and taking summation on i, j over $0 \leq i \leq N_x - 1, 0 \leq j \leq N_y - 1$, we arrive at

$$\begin{aligned} \left(\frac{\Phi^{n+1} - \Phi^n}{\Delta t}, W^{n+1/2} \right)_{l^2, M} & = -\lambda\epsilon^2 (d_x D_x \Phi^{n+1/2} + d_y D_y \Phi^{n+1/2}, \frac{\Phi^{n+1} - \Phi^n}{\Delta t})_{l^2, M} \\ & \quad - \lambda \chi^{*,n+1/2} \left(\bar{f}(\Phi^{*,n+1/2}), \frac{\Phi^{n+1} - \Phi^n}{\Delta t} \right)_{l^2, M} \\ & \quad + \frac{\kappa \lambda \chi^{*,n+1/2}}{\Delta t} (\Phi^{n+1/2} - \Phi^{*,n+1/2}, \Phi^{n+1} - \Phi^n)_{l^2, M}. \end{aligned}$$

Recalling Lemma 3.1, we rewrite the first term on the right-hand side of (3.28) as

$$\begin{aligned} & - (d_x D_x \Phi^{n+1/2} + d_y D_y \Phi^{n+1/2}, \frac{\Phi^{n+1} - \Phi^n}{\Delta t})_{l^2, M} \\ & = (D_x \Phi^{n+1/2}, \frac{D_x \Phi^{n+1} - D_x \Phi^n}{\Delta t})_{l^2, T, M} + (D_y \Phi^{n+1/2}, \frac{D_y \Phi^{n+1} - D_y \Phi^n}{\Delta t})_{l^2, M, T} \\ & = \frac{\|\mathbf{D}\Phi^{n+1}\|_{l^2}^2 - \|\mathbf{D}\Phi^n\|_{l^2}^2}{2\Delta t}. \end{aligned}$$

Now combining the above identities we obtain

$$\begin{aligned} \left(\frac{\Phi^{n+1} - \Phi^n}{\Delta t}, W^{n+1/2} \right)_{l^2, M} &= \frac{\|\mathbf{D}\Phi^{n+1}\|_{l^2}^2 - \|\mathbf{D}\Phi^n\|_{l^2}^2}{2\Delta t} \\ &\quad - \chi^{*,n+1/2} \left(\tilde{f}(\Phi^{*,n+1/2}), \frac{\Phi^{n+1} - \Phi^n}{\Delta t} \right)_{l^2, M} \\ &\quad + \frac{\kappa \chi^{*,n+1/2}}{\Delta t} (\Phi^{n+1/2} - \Phi^{*,n+1/2}, \Phi^{n+1} - \Phi^n)_{l^2, M}. \end{aligned} \quad (3.28)$$

Multiplying (3.25c) by $(\frac{\tilde{U}_1^{n+1} + U_1^n}{2})_{i,j+1/2} h_x h_y$, and taking summation over i, j for $1 \leq i \leq N_x - 1, 0 \leq j \leq N_y - 1$, we have

$$\begin{aligned} &\frac{1}{2\Delta t} (\|\tilde{U}_1^{n+1}\|_{l^2, T, M}^2 - \|U_1^n\|_{l^2, T, M}^2) + \chi^{*,n+1/2} (C_1^{*,n+1/2}, \frac{\tilde{U}_1^{n+1} + U_1^n}{2})_{l^2, T, M} \\ &\quad + v \left\| \frac{d_x \tilde{U}_1^{n+1} + d_x U_1^n}{2} \right\|_{l^2, M} + v \left\| \frac{D_y \tilde{U}_1^{n+1} + D_y U_1^n}{2} \right\|_{l^2, T_y} \\ &\quad - (P^n, \frac{d_x \tilde{U}_1^{n+1} + d_x U_1^n}{2})_{l^2, M} - (\Pi_h W^{n+1/2} D_x \Phi^{n+1/2}, \frac{\tilde{U}_1^{n+1} + U_1^n}{2})_{l^2, T, M} = 0. \end{aligned} \quad (3.29)$$

Multiplying (3.25d) by $(\frac{\tilde{U}_2^{n+1} + U_2^n}{2})_{i+1/2, j} h_x h_y$, and taking summation over i, j for $0 \leq i \leq N_x - 1, 1 \leq j \leq N_y - 1$ leads to

$$\begin{aligned} &\frac{1}{2\Delta t} (\|\tilde{U}_2^{n+1}\|_{l^2, M, T}^2 - \|U_2^n\|_{l^2, M, T}^2) + \chi^{*,n+1/2} (C_1^{*,n+1/2}, \frac{\tilde{U}_2^{n+1} + U_2^n}{2})_{l^2, M, T} \\ &\quad + v \left\| \frac{d_y \tilde{U}_2^{n+1} + d_y U_2^n}{2} \right\|_{l^2, M} + v \left\| \frac{D_x \tilde{U}_2^{n+1} + D_x U_2^n}{2} \right\|_{l^2, T_x} \\ &\quad - (P^n, \frac{d_y \tilde{U}_2^{n+1} + d_y U_2^n}{2})_{l^2, M} - (\Pi_h W^{n+1/2} D_y \Phi^{n+1/2}, \frac{\tilde{U}_2^{n+1} + U_2^n}{2})_{l^2, M, T} = 0. \end{aligned} \quad (3.30)$$

It follows directly from (3.25e)-(3.25f) that

$$\frac{1}{2\Delta t} \|\mathbf{U}^{n+1} - \tilde{\mathbf{U}}^{n+1}\|_{l^2}^2 = \frac{\Delta t}{8} \|\mathbf{D}P^{n+1} - \mathbf{D}P^n\|_{l^2}^2. \quad (3.31)$$

Taking discrete inner products of (3.25e)-(3.25f) with $U_{1,i,j+1/2}^{n+1} h_x h_y$, $U_{2,i+1/2,j}^{n+1} h_x h_y$ respectively, we obtain

$$\|\mathbf{U}^{n+1}\|_{l^2}^2 - \|\tilde{\mathbf{U}}^{n+1}\|_{l^2}^2 + \|\mathbf{U}^{n+1} - \tilde{\mathbf{U}}^{n+1}\|_{l^2}^2 = 0. \quad (3.32)$$

We further rewrite the projection step (3.25e)-(3.25f) as

$$U_1^{n+1} + U_1^n - (\tilde{U}_1^{n+1} + U_1^n) + \frac{\Delta t}{2} (D_x P^{n+1} - D_x P^n) = 0, \quad (3.33a)$$

$$U_2^{n+1} + U_2^n - (\tilde{U}_2^{n+1} + U_2^n) + \frac{\Delta t}{2} (D_y P^{n+1} - D_y P^n) = 0. \quad (3.33b)$$

Taking discrete inner products of (3.33a) and (3.33b) with $\frac{\Delta t}{2} D_x P_{i+1/2, j+1/2}^n h_x h_y$, $\frac{\Delta t}{2} D_y P_{i+1/2, j+1/2}^n h_x h_y$ respectively, summing them up, after applying the divergence-free condition (3.25g), it is clear that

$$\begin{aligned}
& (D_x P^n, \frac{\tilde{U}_1^{n+1} + U_1^n}{2})_{l^2, T, M} + (D_y P^n, \frac{\tilde{U}_2^{n+1} + U_2^n}{2})_{l^2, M, T} \\
&= \frac{\Delta t}{8} [\|\mathbf{D}P^{n+1}\|_{l^2}^2 - \|\mathbf{D}P^n\|_{l^2}^2 - \|\mathbf{D}P^{n+1} - \mathbf{D}P^n\|_{l^2}^2].
\end{aligned} \quad (3.34)$$

Combining Eqs. (3.27)–(3.32) with (3.34) and (3.25k) and noting (3.25g), similar to that of Theorem 3.1 gives the desired result (3.26).

The uniform upper bound of $\{S^n\}$ can be regarded as a direct result of the energy dissipation, which can be established through a procedure similar to that outlined in the proof of Corollary 3.1. Notice that from Theorem 3.1, we know

$$S^{*,n+\frac{1}{2}} \leq E_h[\Phi^{*,n+\frac{1}{2}}, \mathbf{U}^{*,n+\frac{1}{2}}, S^{*,n+\frac{1}{2}}] \leq E_h[\Phi^n, \mathbf{U}^n, S^n],$$

and hence, we also have $S^{*,n+\frac{1}{2}} \leq \mathcal{E}_h[\Phi_{init}, \mathbf{U}_{init}]$, as $S^{*,n+\frac{1}{2}}$ is generated by the pressure-correction sESAV1 scheme (3.15). \square

Theorem 3.4 (Discrete MBP of the MBP-sESAV2 scheme) *If f be continuously differentiable on $[-\beta, \beta]$ and $\kappa \geq \|f'\|_{C[-\beta, \beta]}$, assume*

$$h \leq \frac{2\lambda\epsilon^2\mathcal{M}}{\hat{C}G^*} \text{ and } \Delta t \leq \left(\frac{G^*\mathcal{M}\lambda\kappa}{2} + \frac{\mathcal{M}\lambda\epsilon^2}{h^2}\right)^{-1}, \quad (3.35)$$

where $\hat{C} > 0$ is defined in Remark 3.2 and $G^* = \exp\{\mathcal{E}_h(\Phi_{init}, \mathbf{U}_{init}) + C_*\}$, then the MBP-sESAV2 scheme (3.25) preserves the MBP unconditionally.

Proof Suppose (Φ^n, S^n) is given and $\|\Phi^n\|_{L^\infty(\Omega)} \leq \beta$ for some n . From (3.25a)–(3.25b), we have

$$\begin{aligned}
\left(\left(\frac{2}{\Delta t} + \mathcal{M}\lambda\kappa\chi^{*,n+1/2}\right)I - \mathcal{L}_{\mathbf{U}^*}\right)\Phi^{n+1} &= \left(\left(\frac{2}{\Delta t} - \mathcal{M}\lambda\kappa\chi^{*,n+1/2}\right)I + \mathcal{L}_{\mathbf{U}^*}\right)\Phi^n \\
&\quad + 2\mathcal{M}\lambda\chi^{*,n+1/2}(\bar{f}(\Phi^{*,n+1/2}) + \kappa\Phi^{*,n+1/2}),
\end{aligned}$$

where

$$\mathcal{L}_{\mathbf{U}^*} = \mathcal{M}\lambda\epsilon^2(d_x D_x + d_y D_y) - \chi^{*,n+1/2} \left(\Pi_h \left(U_1^{*,n+1/2} \right) \nabla_x + \Pi_h \left(U_2^{*,n+1/2} \right) \nabla_y \right).$$

Noticing Theorems 3.1 and 3.3, it follows that $\|\Phi^{*,n+1/2}\|_{L^\infty(\Omega)} \leq \beta$ and $S^{*,n+\frac{1}{2}} \leq \mathcal{E}_h[\Phi_{init}, \mathbf{U}_{init}]$. Consequently, we deduce that $0 < \chi^{*,n+1/2}(\Phi, S) \leq G^*$ through a similar analysis as demonstrated in Theorems 3.2. If the inequality

$$h \max \left\{ \|U_{1,i,j}^{*,n+1/2}\|_{L^\infty}, \|U_{2,i,j}^{*,n+1/2}\|_{L^\infty} \right\} \leq h\hat{C} \leq \frac{2\lambda\epsilon^2\mathcal{M}}{G^*}, \quad (3.36)$$

is satisfied, then $\mathcal{L}_{\mathbf{U}^*}$ is a negative diagonally dominant matrix, and the coefficient matrix of (3.25a)–(3.25b) satisfies the conditions of Lemma 2.1. Now (3.35) implies

$$\frac{2}{\Delta t} - \mathcal{M}\lambda\kappa\chi^{*,n+1/2} \geq \frac{2\mathcal{M}\lambda\epsilon^2}{h^2}.$$

Note that

$$\left\| \left(\frac{2}{\Delta t} - \mathcal{M}\lambda\kappa\chi^{*,n+1/2} \right) I + \mathcal{L}_{\mathbf{U}^*} \right\|_{L^\infty(\Omega)} = \frac{2}{\Delta t} - \mathcal{M}\lambda\kappa\chi^{*,n+1/2}.$$

Due to $\kappa \geq \|f'\|_{C[-\beta, \beta]}$ and Lemma 2.2, we have $\|\bar{f}(\Phi^{*,n+1/2}) + \kappa \Phi^{*,n+1/2}\|_{L^\infty(\Omega)} \leq \kappa\beta$. Thus, under the condition specified in (3.35) and using Lemma 2.1, we derive

$$\begin{aligned} \|\Phi^{n+1}\|_{L^\infty(\Omega)} &\leq \left(\frac{2}{\Delta t} + \mathcal{M}\lambda\kappa\chi^{*,n+1/2}\right)^{-1} \\ &\quad \left[\left(\frac{2}{\Delta t} - \mathcal{M}\lambda\kappa\chi^{*,n+1/2}\right)\beta + 2\mathcal{M}\kappa\lambda\chi^{*,n+1/2}\beta\right] = \beta, \end{aligned}$$

then we have $\|\Phi^n\|_{L^\infty(\Omega)} \leq \beta$ by induction for all n . \square

Remark 3.4 The condition given by (3.35) on the time step size implies that $\Delta t = O(h^2/\mathcal{M}\lambda\epsilon^2)$. In practical computations, we observe that $\chi^{*,n+1/2} \approx 1$, which allows us to set a requirement for the time step size as $\Delta t \leq (\frac{\mathcal{M}\lambda\kappa}{2} + \frac{\mathcal{M}\lambda\epsilon^2}{h^2})^{-1}$ in order to preserve the MBP, as utilized in our subsequent numerical experiments.

4 Numerical Simulations

In this section, we provide some numerical experiments to validate our theoretical results and the MBP-preserving properties of the constructed schemes for the conserved ACNS model. Unless otherwise specified, we adopt $C_* = 1$ and the Flory-Huggins potential (2.6) with the parameters $\theta = 0.8$ and $\theta_c = 1.6$ for the simulation. If f is the double-well potential function (2.5), we choose $\kappa = 3$ as the stabilizing coefficient, whereas if it is the Flory-Huggins potential function (2.6), we set $\kappa = 28.87$. In addition, we take $\sigma(x) = \exp(x)$ for $\sigma(x)$ in (2.12).

4.1 Convergence Tests

We test the convergence in two dimensions, with the Flory-Huggins potential function f defined in (2.5). The model parameters are taken as follows:

$$\mathcal{M} = 0.001, \quad \lambda = 2, \quad \epsilon^2 = 0.1, \quad \nu = 0.1, \quad L_x = L_y = 1, \quad \kappa = 0.$$

We choose right-hand sides of (1.1) suitably such that the exact solution is given by:

$$\begin{aligned} \phi(x, y, t) &= \cos(t) \cos(\pi x) \cos(\pi y), \\ \mathbf{u}(x, y, t) &= 0.1 \sin(t) (\sin^2(\pi x) \sin(2\pi y), -\sin(2\pi x) \sin^2(\pi y)), \\ p(x, y, t) &= \sin(t) (\sin(\pi y) - 2/\pi). \end{aligned}$$

Example 1 (Refinement in space) We first test convergence rates the of the first- and second-order schemes in space. The reference solution is computed using the time step of $\Delta t = 10^{-5}$. The errors at $T = 0.5$, measured in the L^2 norm with varying space steps, are presented in Fig. 1, distinctly demonstrating the second-order convergence in the spatial dimension.

Example 2 (Refinement in time) Next, we use 256×256 modes to discretize the space variables so that the spatial discretization error is negligible compared to the time discretization. In Fig. 2, we list the errors of the phase variable ϕ , the velocity \mathbf{u} , and the pressure p between the numerical and the exact solution at $T = 0.128$. It can be observed that our schemes match the expected accuracy in time perfectly well.

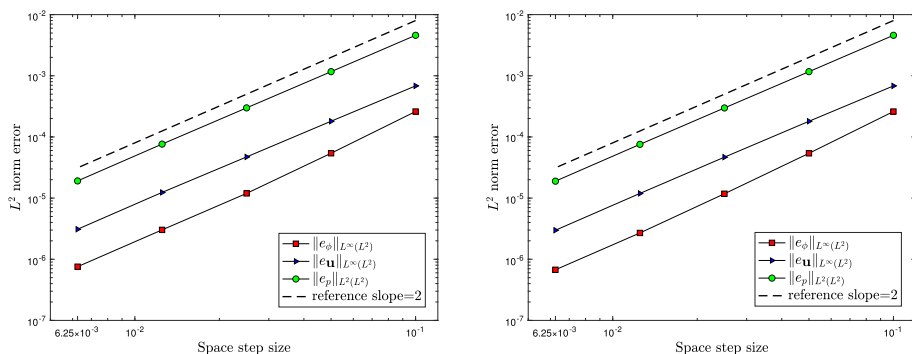


Fig. 1 Numerical convergence rate of the first-(left) and second-order schemes (right)

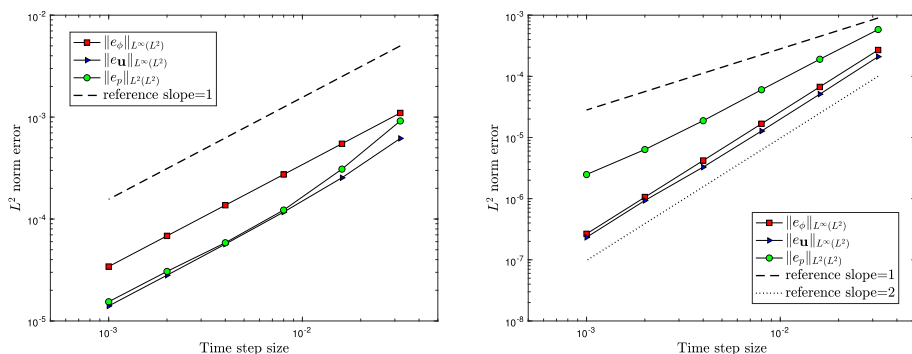


Fig. 2 Numerical convergence rate of the first-(left) and second-order schemes (right)

4.2 MBP Tests for the Flow-Coupled Phase Separation

In this example, we perform the numerical simulations of spinodal decomposition in a two-dimensional setting. The simulations are carried out on $[0, L]^2$ with $L = 1.0$. We test the MBP-sESAV2 scheme with a spatial mesh size of $h = 1/100$ and a time step size $\Delta t = 10^{-3}$.

The initial condition is a random state, in which a random number ranging from -0.9 to 0.9 is assigned to each grid point. Moreover, both the double-well potential function (2.5) and the Flory-Huggins potential function (2.6) are discussed here. We choose the parameters for Fig. 3 and Fig. 4a–c as follows:

$$\mathcal{M} = 0.5, \quad \lambda = 100, \quad \epsilon = 0.01, \quad \nu = 1.0. \quad (4.39)$$

In Fig. 3, a comparison of two simulations produced by the two different potentials shows that the evolution processes are overall similar. It can be observed that the discrete MBP holds, and the energy decays monotonically with time in Fig. 4a–c. The red solid lines represent $y = \beta = 2\sqrt{3}/3$ and $y = \beta \approx 0.9868$, respectively, which are the theoretical maximum bound [18, 27] for the double-well potential function and the Flory-Huggins potential function. In Fig. 4d, we investigate unconditional stability by setting $\mathcal{M} = 0.15$, $\lambda = 100$, $\epsilon = 0.03$, $\nu = 1.0$ and $\kappa = 0$ with MBP-sESAV1 scheme, while employing various time step sizes with $\Delta t = 1, 0.1, 0.01$. Our results confirm that the modified energy consistently decreases, as demonstrated in Theorem 3.1 and Theorem 3.3. In addition, we observe that

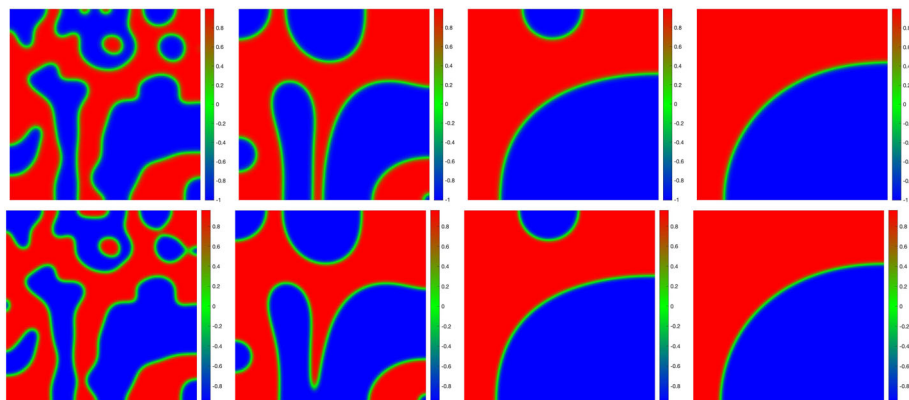


Fig. 3 Snapshots of the phase function ϕ at $t = 0.2, 1.1, 5, 10$ for the ACNS model (1.1) with the double-well potential (top) and the Flory-Huggins potential (bottom) in two dimensions

the original energy oscillates slightly with $\Delta t = 1$, while the modified energy consistently shows a decreasing trend. This further validates that our scheme can achieve modified energy dissipation even with large time steps.

4.3 Shape Relaxation

In this simulation, we adopt a star-shaped interface evolution with the initial value given by

$$\begin{aligned} \phi(x, y, 0) &= 0.9 \tanh \frac{0.25 + 0.1 \cos(a\theta) - r}{\sqrt{2}\epsilon}, \\ \theta &= \arctan \frac{y - 0.5}{x - 0.5}, \quad r = \sqrt{(x - 0.5)^2 + (y - 0.5)^2}. \end{aligned} \quad (4.40)$$

The parameter a represents the number of vertices of the initial data. We discretize the space variables with 100×100 modes, and choose the values of parameters as

$$\Delta t = 0.001, \quad \lambda = 100, \quad \mathcal{M} = 0.5, \quad \epsilon = 0.01, \quad \nu = 1.0, \quad L_x = L_y = 1.0.$$

In Fig. 5, we depict the dynamic process of shape relaxation towards a disk by setting different values of a in (4.40). As indicated in [41–43], it can be clearly observed from Fig. 6 that the larger value of a (indicating more vertices of the initial data), the faster rate of the evolution process, which is consistent with the findings in Fig. 5. It appears that the interfacial thickness, approximated to the distance between contours $\phi = -0.8$ and $\phi = 0.8$, remains constant with different a . The evolutions of the supremum norm of ϕ and the energy of the simulated solutions are displayed in Fig. 6. One can also observe that the discrete MBP is well preserved, and the energy decays monotonically.

4.4 Buoyancy-Driven Flow

In this example, we modify the momentum Eq. (1.1c) by adding the following buoyancy term on the right-hand side of (1.1c)

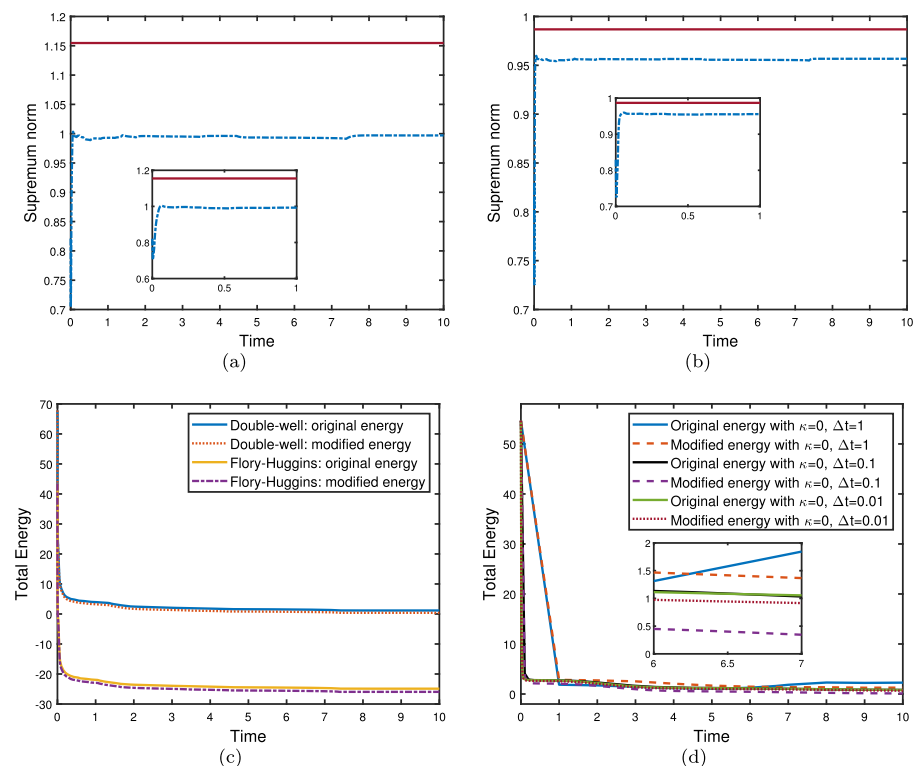


Fig. 4 Evolutions of the supremum norm (a)(b) and energies (c) for the ACNS model (1.1) with both the double-well potential (2.5) and the Flory-Huggins potential (2.6). d depicts the evolution of energies for the double-well potential (2.5)

$$b(\phi)\mathbf{g} = G(\rho(\phi) - \bar{\rho})\mathbf{g} = G \frac{\phi_1 - \phi_2}{2}(\phi - \bar{\phi})\mathbf{g} := \chi(\phi - \bar{\phi})\mathbf{g}, \quad \mathbf{g} = (0, 1)^T,$$

where $\bar{\phi}$ represents the spatially averaged parameter. Thus one obtains

$$\frac{\partial \mathbf{u}}{\partial t} + \mathbf{u} \cdot \nabla \mathbf{u} - \nu \Delta \mathbf{u} + \nabla p = \mu \nabla \phi + \chi(\phi - \bar{\phi})\mathbf{g}. \quad (4.41)$$

The computational domain is $\Omega = [0, 1]^2$, and we use 100×100 modes to discretize the space variables. The numerical parameters are set as follows:

$$\Delta t = 0.001, \quad \lambda = 10, \quad \epsilon = 0.01.$$

Example 3 (Bubble rising) The phase function is initialized with a circular bubble positioned at the center of the domain at the coordinates $(0.5, 0.25)$, and the initial velocity is set to $u_0 = 0$. The top pictures given in Fig. 7 present snapshots of the phase evolution at different time points ($t = 1.0, 6.0, 10.0, 13.1$). Initially, the bubble is observed as a circular shape located near the lower region of the domain. As the bubble, which possesses a lower density compared to the surrounding fluid, rises gradually, it undergoes a transition into an elliptical shape and eventually deforms as it approaches the upper boundary, as expected in the reference [34]. Additionally, streamline visualizations of velocities are provided in the bottom of Fig. 7.

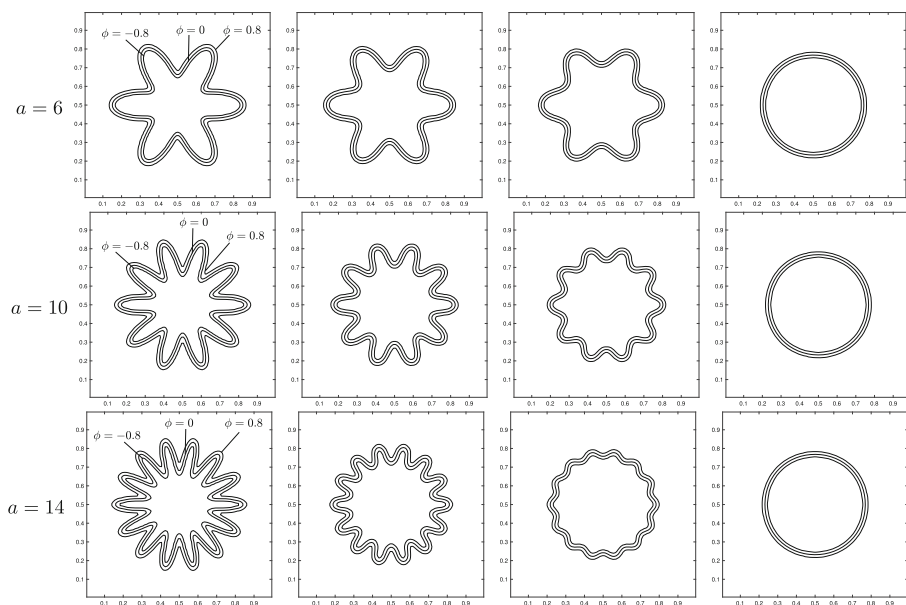


Fig. 5 Snapshots of the phase function ϕ with contours $\phi = -0.8, 0, 0.8$ for $a = 6, 10, 14$ at $t = 0.01, 0.1, 0.2, 1$ respectively

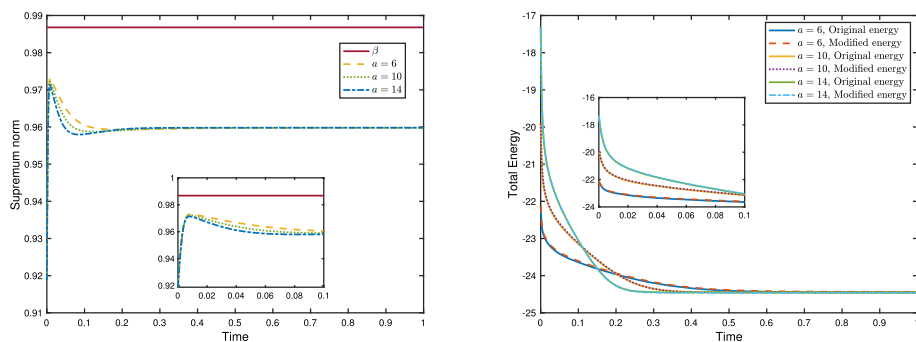


Fig. 6 Time evolutions of supremum norms (left) and energies(right) for different a

Example 4 (Dripping droplet) We commence by conducting simulations to investigate the dynamic behavior of a dripping droplet under different Reynolds numbers, namely $\nu = 1/10$ and $1/20$. Initially, the droplet, which has a heavier density compared to its surrounding medium (e.g., air), adheres to the upper solid wall. Due to the influence of gravity with $\chi = 50$, the droplet gradually falls. In Fig. 8, the first row displays the snapshots of the droplet for $\nu = 1/10$, while the top row in Fig. 9 depicts the evolution results for $\nu = 1/20$. It is evident that as the Reynolds number $1/\nu$ increases, the pinch-off process occurs more rapidly and the droplet falls more quickly. Furthermore, the velocity streamlines are presented in the bottom row of Figs. 8 and 9. It can be seen that the formation of spike structures becomes more evident, especially when the liquid filament is extensively elongated. These simulations are consistent with the experimental presented in [44] and the simulations demonstrated in [5, 45]. High temporal accuracy can be achieved in the MBP-sESAV2 scheme by utilizing

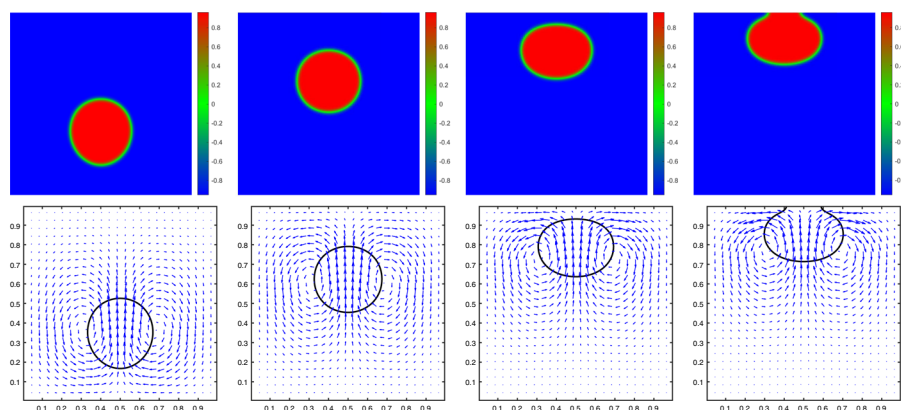


Fig. 7 Snapshots of the phase function ϕ (top) and velocity field (bottom) with $\nu = 1$, $\chi = 10$ and $\mathcal{M} = 5.0$ for bubble rising at different time $t = 1.0, 6.0, 10.0, 13.1$

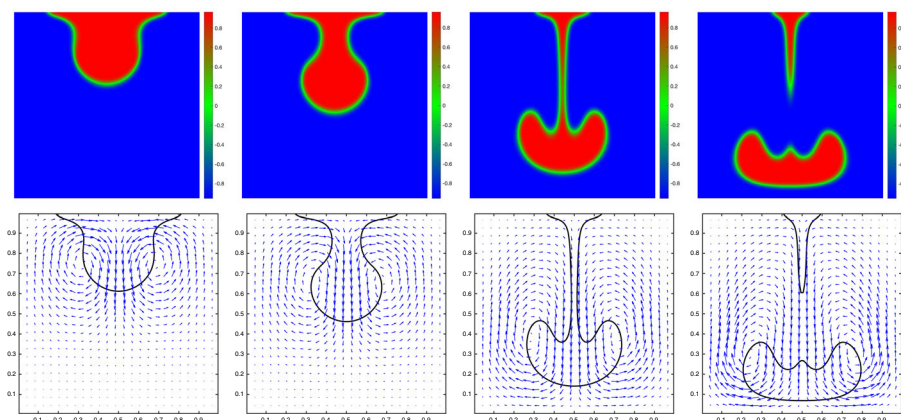


Fig. 8 Snapshots of the phase function ϕ (top) and velocity field (bottom) with $\nu = 0.1$ and $\mathcal{M} = 1.0$ for dripping droplet at different time $t = 0.2, 0.3, 0.5, 0.6$

a time step $\Delta t = 0.001$, which is a noteworthy result. In Fig. 10, we again observe that the MBP for the ACNS model with (4.41) is numerically well-preserved.

5 Concluding Remarks

We develop efficient numerical schemes, both first- and second-order, to solve the hydrodynamically coupled mass-conserved Allen-Cahn phase-field model for a two-phase flow system. These schemes are constructed by combining the projection method for the Navier-Stokes equation and the generalized stabilized exponential scalar auxiliary variable approach for the decoupling of the nonlinear terms. The proposed schemes possess several desirable properties, including linearity, second-order accuracy in space and time, complete decoupling and particularly the preservation of the MBP. In addition, we also demonstrate the unconditional energy dissipation based on the generalized stabilized exponential scalar auxiliary

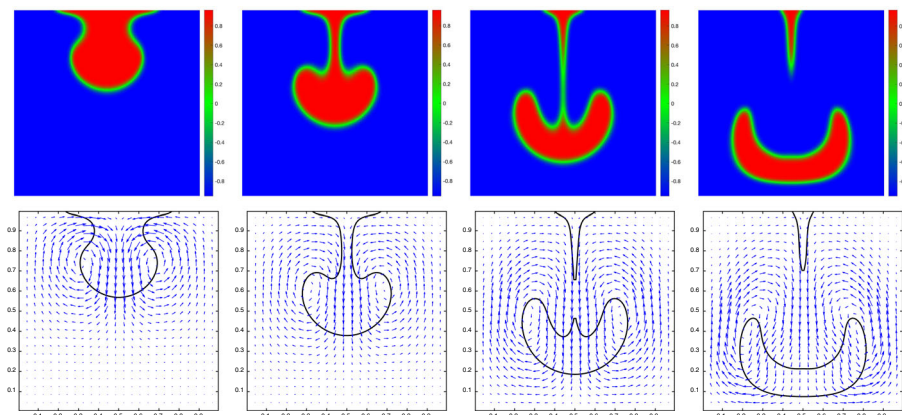


Fig. 9 Snapshots of the phase function ϕ (top) and velocity field (bottom) with $\nu = 0.05$ and $\mathcal{M} = 1.0$ for dripping droplet at different time $t = 0.2, 0.3, 0.4, 0.5$

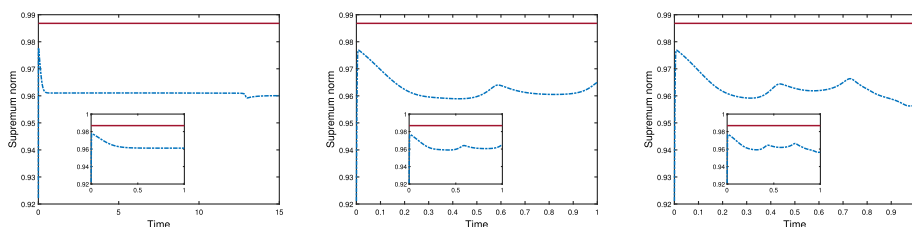


Fig. 10 Time evolutions of supremum norms: bubble rising with $\nu = 1$, $\chi = 10$ (left), dripping droplet with $\nu = 0.1$, $\chi = 50$ (middle), and $\nu = 0.05$, $\chi = 50$ (right)

variable approach. Furthermore, we provide a rigorous proof of the preservation of the MBP for both schemes.

Acknowledgements The authors are grateful to Professor X. Zhang of Purdue University for helpful discussions.

Funding Open access funding provided by The Hong Kong Polytechnic University. X. Li is supported in part by the National Natural Science Foundation of China (Grant Nos. 12271302, 12131014) and Shandong Provincial Natural Science Foundation for Outstanding Youth Scholar (Grant No. ZR2024JQ030). N. Zheng is partially supported by the Hong Kong Polytechnic University Postdoctoral Research Fund 1-W22P and CAS AMSS-PolyU Joint Laboratory of Applied Mathematics.

Data availability All data included in this study are available upon request by contact with the corresponding author.

Declarations

Conflict of interest The authors have not disclosed any Conflict of interest.

Open Access This article is licensed under a Creative Commons Attribution 4.0 International License, which permits use, sharing, adaptation, distribution and reproduction in any medium or format, as long as you give appropriate credit to the original author(s) and the source, provide a link to the Creative Commons licence, and indicate if changes were made. The images or other third party material in this article are included in the article's Creative Commons licence, unless indicated otherwise in a credit line to the material. If material is not included in the article's Creative Commons licence and your intended use is not permitted by statutory

regulation or exceeds the permitted use, you will need to obtain permission directly from the copyright holder. To view a copy of this licence, visit <http://creativecommons.org/licenses/by/4.0/>.

References

- Diegel, A.E., Wang, C., Wang, X., Wise, S.M.: Convergence analysis and error estimates for a second order accurate finite element method for the Cahn-Hilliard-Navier-Stokes system. *Numer. Math.* **137**, 495–534 (2017)
- Jeong, D., Kim, J.: Conservative Allen-Cahn-Navier-Stokes system for incompressible two-phase fluid flows. *Comput. & Fluids* **156**, 239–246 (2017)
- Kay, D., Welford, R.: Efficient numerical solution of Cahn-Hilliard-Navier-Stokes fluids in 2D. *SIAM J. Sci. Comput.* **29**(6), 2241–2257 (2007)
- Tsuzuki, R., Li, Q., Nagatsu, Y., Chen, C.-Y.: Numerical study of immiscible viscous fingering in chemically reactive Hele-Shaw flows: production of surfactants. *Phys. Rev. Fluids* **4**(10), 104003 (2019)
- Yang, X.: A novel fully decoupled scheme with second-order time accuracy and unconditional energy stability for the Navier-Stokes equations coupled with mass-conserved Allen-Cahn phase-field model of two-phase incompressible flow. *Int. J. Numer. Meth. Eng.* **122**(5), 1283–1306 (2021)
- Rubinstein, J., Sternberg, P.: Nonlocal reaction-diffusion equations and nucleation. *IMA J. Appl. Math.* **48**(3), 249–264 (1992)
- Shen, J.: On error estimates of projection methods for Navier-Stokes equations: first-order schemes. *SIAM J. Numer. Anal.* **29**(1), 57–77 (1992)
- Shen, J.: Modeling and numerical approximation of two-phase incompressible flows by a phase-field approach, In: *Multiscale modeling and analysis for materials simulation*, world scientific 147–195 (2012)
- Liu, C., Shen, J., Yang, X.: Dynamics of defect motion in nematic liquid crystal flow: modeling and numerical simulation. *Commun. Comput. Phys.* **2**(6), 1184–1198 (2007)
- Shen, J., Wang, C., Wang, X., Wise, S.M.: Second-order convex splitting schemes for gradient flows with Ehrlich-Schwoebel type energy: application to thin film epitaxy. *SIAM J. Numer. Anal.* **50**(1), 105–125 (2012)
- Wang, C., Wise, S.M.: An energy stable and convergent finite-difference scheme for the modified phase field crystal equation. *SIAM J. Numer. Anal.* **49**(3), 945–969 (2011)
- Yang, X., Zhao, J., Wang, Q.: Numerical approximations for the molecular beam epitaxial growth model based on the invariant energy quadratization method. *J. Comput. Phys.* **333**, 104–127 (2017)
- Yang, X., Zhang, G.-D.: Convergence analysis for the invariant energy quadratization (IEQ) schemes for solving the Cahn-Hilliard and Allen-Cahn equations with general nonlinear potential. *J. Sci. Comput.* **82**, 1–28 (2020)
- Shen, J., Xu, J.: Convergence and error analysis for the scalar auxiliary variable (SAV) schemes to gradient flows. *SIAM J. Numer. Anal.* **56**(5), 2895–2912 (2018)
- Shen, J., Xu, J., Yang, J.: A new class of efficient and robust energy stable schemes for gradient flows. *SIAM Rev.* **61**(3), 474–506 (2019)
- Shen, J., Tang, T., Yang, J.: On the maximum principle preserving schemes for the generalized Allen-Cahn equation. *Commun. Math. Sci.* **14**(6), 1517–1534 (2016)
- Cai, Y., Ju, L., Lan, R., Li, J.: Stabilized exponential time differencing schemes for the convective Allen-Cahn equation. *Commun. Math. Sci.* **21**(1), 127–150 (2023)
- Lan, R., Li, J., Cai, Y., Ju, L.: Operator splitting based structure-preserving numerical schemes for the mass-conserving convective Allen-Cahn equation. *J. Comput. Phys.* **472**, 111695 (2023)
- Huang, Z., Lin, G., Ardekani, A.M.: Consistent and conservative scheme for incompressible two-phase flows using the conservative Allen-Cahn model. *J. Comput. Phys.* **420**, 109718 (2020)
- Ju, L., Li, X., Qiao, Z.: Generalized SAV-exponential integrator schemes for Allen-Cahn type gradient flows. *SIAM J. Numer. Anal.* **60**(4), 1905–1931 (2022)
- Ju, L., Li, X., Qiao, Z.: Stabilized exponential-SAV schemes preserving energy dissipation law and maximum bound principle for the Allen-Cahn type equations. *J. Sci. Comput.* **92**(1), 1–34 (2022)
- Hu, J., Zhang, X.: Positivity-preserving and energy-dissipative finite difference schemes for the Fokker-Planck and Keller-Segel equations. *IMA J. Numer. Anal.* **43**(3), 1450–1484 (2023)
- Li, H., Zhang, X.: On the monotonicity and discrete maximum principle of the finite difference implementation of C^0 - Q^2 finite element method. *Numer. Math.* **145**, 437–472 (2020)
- Ma, D.: Classical solutions to a model of two-phase incompressible flows with variable density. *J. Math. Anal. Appl.* **525**(2), 127158 (2023)

25. Medjo, T.T., Tone, C., Tone, F.: Long-time stability of the implicit Euler scheme for a three dimensional globally modified two-phase flow model. *Asymptot. Anal.* **118**(3), 161–208 (2020)
26. Chipot, M.: *Handbook of differential equations: stationary partial differential equations*, Elsevier (2011)
27. Li, J., Ju, L., Cai, Y., Feng, X.: Unconditionally maximum bound principle preserving linear schemes for the conservative Allen-Cahn equation with nonlocal constraint. *J. Sci. Comput.* **87**, 1–32 (2021)
28. Alfaro, M., Alifrangis, P.: Convergence of a mass conserving Allen-Cahn equation whose lagrange multiplier is nonlocal and local. *Interfaces Free. Boundaries* **16**(2), 243–268 (2014)
29. Brassel, M., Bretin, E.: A modified phase field approximation for mean curvature flow with conservation of the volume. *Math. Methods Appl. Sci.* **10**(34), 1157–1180 (2011)
30. Jiang, K., Ju, L., Li, J., Li, X.: Unconditionally stable exponential time differencing schemes for the mass-conserving Allen-Cahn equation with nonlocal and local effects. *Numer. Methods Part. Differ. Equ.* **38**(6), 1636–1657 (2022)
31. Kim, J., Lee, S., Choi, Y.: A conservative Allen-Cahn equation with a space-time dependent lagrange multiplier. *Int. J. Eng. Sci.* **84**, 11–17 (2014)
32. Cheng, Q., Liu, C., Shen, J.: Generalized SAV approaches for gradient systems. *J. Comput. Appl. Math.* **394**, 113532 (2021)
33. Rui, H., Li, X.: Stability and superconvergence of MAC scheme for Stokes equations on nonuniform grids. *SIAM J. Numer. Anal.* **55**(3), 1135–1158 (2017)
34. Li, X., Shen, J.: On a SAV-MAC scheme for the Cahn-Hilliard-Navier-Stokes phase-field model and its error analysis for the corresponding Cahn-Hilliard-Stokes case. *Math. Models Methods Appl. Sci.* **30**(12), 2263–2297 (2020)
35. Van Kan, J.: A second-order accurate pressure-correction scheme for viscous incompressible flow. *SIAM J. Sci. Stat. Comput.* **7**(3), 870–891 (1986)
36. Shen, J.: On error estimates of the projection methods for the Navier-Stokes equations: second-order schemes. *Math. Comput.* **65**(215), 1039–1065 (1996)
37. Weinan, E., Liu, J.-G.: Projection method I: convergence and numerical boundary layers, *SIAM J. Numer. Anal.* 1017–1057 (1995)
38. Guermond, J., Shen, J.: On the error estimates for the rotational pressure-correction projection methods. *Math. Comput.* **73**(248), 1719–1737 (2004)
39. Han, D., Wang, X.: A second order in time, uniquely solvable, unconditionally stable numerical scheme for Cahn-Hilliard-Navier-Stokes equation. *J. Comput. Phys.* **290**, 139–156 (2015)
40. Guermond, J.-L., Mineev, P., Shen, J.: An overview of projection methods for incompressible flows. *Comput. Methods Appl. Mech. Eng.* **195**(44–47), 6011–6045 (2006)
41. Wise, S.M.: Unconditionally stable finite difference, nonlinear multigrid simulation of the Cahn-Hilliard-Hele-Shaw system of equations. *J. Sci. Comput.* **44**(1), 38–68 (2010)
42. Han, D., Wang, X.: A second order in time, decoupled, unconditionally stable numerical scheme for the Cahn-Hilliard-Darcy system. *J. Sci. Comput.* **77**, 1210–1233 (2018)
43. Zheng, N., Li, X.: Error analysis of the SAV Fourier-spectral method for the Cahn-Hilliard-Hele-Shaw system. *Adv. Comput. Math.* **47**, 1–27 (2021)
44. Bonhomme, R., Magnaudet, J., Duval, F., Piar, B.: Inertial dynamics of air bubbles crossing a horizontal fluid-fluid interface. *J. Fluid Mech.* **707**, 405–443 (2012)
45. Tirtaatmadja, V., McKinley, G.H., Cooper-White, J.J.: Drop formation and breakup of low viscosity elastic fluids: effects of molecular weight and concentration. *Physics of Fluids* (2006). <https://doi.org/10.1063/1.2190469>